ERASMUS, RUDOLPH MARTHINUS

METASTABLE DEFECTS IN ALPHAPARTICLE IRRADIATED n-GaAs

MSc UP 1997

Metastable defects in alpha–particle irradiated n-GaAs

by

Rudolph Marthinus Erasmus

Submitted in partial fulfilment of the requirements for the degree

MSc (Physics)

in the

Faculty of Science

University of Pretoria

Pretoria

March 1997

Supervisor: Prof F D Auret

Co-supervisor: Dr S A Goodman

Metastable defects in alpha–particle irradiated n-GaAs

by

Rudolph Marthinus Erasmus

Submitted in partial fulfilment of the requirements for the degree

MSc (Physics)

in the

Faculty of Science

University of Pretoria

Supervisor: Prof F D Auret

Co-supervisor: Dr S A Goodman

The controlled introduction of defects in semiconductors by means of different types of irradiation, is a well-established technique in the study of semiconductor structures. It has application in the study of defects introduced in semiconductors in a radiation environment. One of the types of radiation readily encountered in a radiation environment, is alpha(α)-particle radiation, thus the influence of these particles on the electronic properties of semiconductors, and thus also GaAs, needs to be investigated.

In this dissertation, the characteristics of a specific defect, termed Eα3, are researched and presented and we argue that it exhibits a metastable character. Along with Eα3, another less prominent defect, termed Eα8, was also found to be metastable. The presence of a metastable defect in a particular radiation environment has important consequences for the technological properties of the semiconductor host and thus for the design of devices on GaAs exposed to alpha particles.

(148 words)

Metastabiele defekte in alpha–partikel bestraalde n-GaAs

deur

Rudolph Marthinus Erasmus

Voorgelê ter gedeeltelike vervulling van die vereistes vir die graad

MSc (Fisika)

aan die

Fakulteit Natuurwetenskappe

Universiteit van Pretoria

Studieleier: Prof F D Auret

Mede-studieleier: Dr S A Goodman

Die beheerde indusering van defekte in halfgeleiers deur middel van verskillende stralingstipes, is 'n welbekende tegniek in die studie van halfgeleierstrukture. Dit het toepassing in die studie van defekte geïnduseer in halfgeleiers in 'n stralingsomgewing. Alpha(α)-deeltjie straling is redelik algemeen aanwesig in stralingsomgewings, dus is die ondersoek van die invloed van hierdie deeltjies op die elektroniese eienskappe van halfgeleiers, en dus ook GaAs, van belang.

In hierdie verhandeling word die karakteristieke van 'n spesifieke defek, aangedui met Eα3, nagevors en gerapporteer. Argumente word voorgelê dat Eα3 metastabiele karakteristieke besit. 'n Tweede, minder prominente defek, aangedui met Eα8, is ook gevind metastabiel te wees. Die teenwoordigheid van ‘n metastabiele defek in 'n spesifieke stralingsomgewing het belangrike implikasies vir die tegnologiese eienskappe van halfgeleiers en dus vir die ontwerp van toestelle op GaAs blootgestel aan alpha-deeltjie straling.

(135 woorde)

Acknowledgements

I would like to thank the following persons sincerely for their contribution towards the completion of this study:

My supervisor, Prof. F.D. Auret, for his enthusiasm for physics, his interest, support and guidance.

My co-supervisor, Dr. S.A. Goodman, for his willingness to help and his example as a dedicated young researcher.

Mr. Walter Meyer for countless suggestions on how to make recalcitrant equipment perform up to and beyond specification and for his probing constructive criticism.

The Foundation for Research Development of South Africa for their financial assistance during this study.

The staff of the Physics Department of the University of Pretoria for their willingness to help, their interest and encouragement.

My family for their unfailing support, interest and encouragement.

Contents

Chapter 1: Introduction

Defects in the crystal lattice of semiconductors are always present, whether introduced in the bulk during material growth and material processing or at the surface and interfaces during the various steps necessary in device manufacture. These defects play a major role in the determination of the electronic properties of semiconductor material because they interact with free carriers and their influence is significant even when their concentrations are very small compared to the free carrier concentration. The characteristics of manufactured devices are on their part again very sensitive to the electronic properties of semiconductor material.

For this reason the identification and characterisation of defects in semiconductors, as well as the understanding of their electronic and thermodynamic properties, are very important and remain an active field of research, also in the case of GaAs.

One of the tools of a physicist to study the structure of semiconductor material, is the controlled introduction of defects in semiconductors by means of different types of irradiation, e.g. the study of vacancy-interstitial pairs in the As sublattice in GaAs by means of electron irradiation (Pons *et al* 1985). Once the defects introduced in a controlled manner have been characterised and identified, it is possible to engineer devices exposed to a radiation environment like outer space so that they are more resistant to the ravages of incoming radiation.

One of the types of radiation readily encountered in a radiation environment, is alpha(α)–particle radiation, thus the influence of these particles on the electronic properties of GaAs also needs to be investigated. In the course of studying α-particle irradiated GaAs by means of deep level transient spectroscopy (DLTS), our research group observed a major defect peak in the DLTS spectrum with a peculiar characteristic: the defect's appearance seemed to depend very specifically on the measurement conditions.

In this dissertation, the characteristics of this defect, termed Eα3, are researched and presented and we argue that it exhibits a metastable character. Along with Eα3, another less prominent defect, termed Eα8, was also found to be metastable. Since the electronic and optical properties of the metastable state differ from that of the stable state, the presence of a metastable defect has

important consequences for the technological properties of the semiconductor host. As a rule, this is undesirable. It is important that a device have steady, reproducible properties. On the other hand, controllable metastability could conceivably be used to tune certain device characteristics, for example as a memory device. Thus because of its metastable character and its prominence in alpha-particle irradiated GaAs, Eα3 has important implications for the design of devices exposed to alpha-particle irradiation.

Up to now, metastable defects have been observed in as-grown GaAs (Buchwald *et al* 1989), as well as in hydrogen- (Leitch *et al* 1991) and deuterium-passivated (Leitch *et al* 1992) epitaxially grown GaAs. Investigations of metastable defects introduced in Si and InP by electron irradiation have been reported by Chantre *et al* (1986) and Levinson *et al* (1983), respectively. Recent reports by Kol'chenko *et al* (1994) and Hesse *et al* (1994) indicate that electron irradiation also introduces metastable defects in GaAs. Although it has been well established that heavier particle irradiation introduces electron and hole defects in GaAs (Pons *et al* 1985), only Auret *et al* (1994) have so far reported on metastable defects introduced by heavier particle irradiation.

It is thus apparent that irradiation induced defects in semiconductors that exhibit a metastable character have given rise to much interest and study. This phenomenon presents a challenging scientific puzzle and this dissertation attempts to add a piece to the puzzle.

In chapters 2 to 6 a short summary is given of the topics in the field of semiconductors that directly apply to this dissertation. In chapter 7 the method followed in the experimental work is described and the results are presented and discussed in chapter 8. Conclusions are contained in chapter 9 together with suggestions for further study.

Chapter 2: Schottky-diode theory

The rectifying properties of metal-semiconductor contacts have been known since the late 19th century, but it was only in 1938 that Schottky (Schottky 1938) and Mott (Mott 1938) independently came up with the explanation of drift and diffusion of electrons over a potential barrier to account for the rectifying behaviour. They each proposed a different mechanism to account for the existence of the potential barrier and the mechanism proposed by Schottky has been shown to best explain the barrier. In this chapter a brief summary of Schottky-diode theory is given as Schottky Barrier Diodes (SBDs) were the type of rectifying contact used in this study. Emphasis is placed on minority carrier injection, since this technique features prominently in this study.

2.1 The structure of a Schottky barrier

When a metal contact is deposited on a semiconductor surface, a potential barrier is set up between the metal and the semiconductor. This potential barrier is called the Schottky barrier and the whole structure is called a Schottky Barrier Diode, since the potential barrier gives diode properties to the metal-semiconductor interface. In practice there is often a thin interfacial layer about 10-20 Å thick, comprised of oxides and impurities like carbon and oxygen, present between the metal and the semiconductor.

2.2 The formation of a Schottky barrier

We first need to define the work function of a solid. The work function of a metal ϕ_m is the amount of energy required to raise an electron from the Fermi level (E_F^m) to a state of rest outside the surface of the metal (the so-called vacuum level). The work function of a semiconductor ϕ_s is the difference in energy between the Fermi level (E_F^s) and the vacuum level. Also important is the electron affinity χ_s of a semiconductor. This is the difference in energy between an electron at rest outside the surface and an electron at the bottom of the conduction band just inside the surface. These quantities are illustrated in figure 2.1(a).

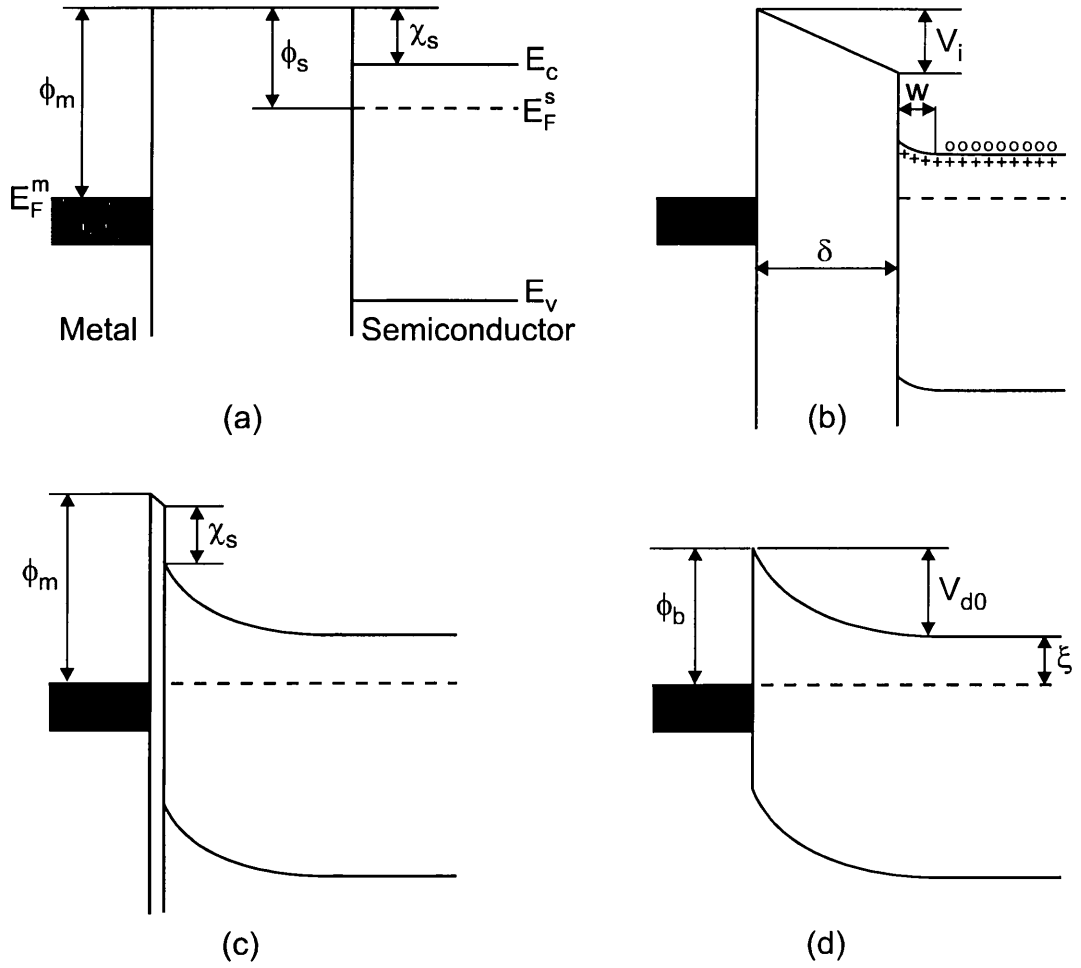

Figure 2.1: Formation of a barrier between a metal and a semiconductor; + denotes a donor ion and o *denotes an electron in the conduction band.*

To illustrate how a Schottky barrier may form when a metal comes into contact with a semiconductor, suppose that the metal and semiconductor are both electrically neutral and separated form each other. This is the case in figure 2.1(a) for an *n*-type semiconductor with a work function less than that of the metal. This is the most important case in practice. If the metal and semiconductor are connected electrically by a wire, electrons pass from the semiconductor into the metal and the two Fermi levels are forced into coincidence as shown in figure 2.1(b). The energies of electrons at rest outside the surfaces of the two solids are no longer the same and there is an electric field in the gap directed from right to left. There must be a negative charge on the surface of the metal balanced by a positive charge in the semiconductor. Since the semiconductor is *n*-type, the positive charge will be provided by conduction electrons receding

from the surface, leaving uncompensated positive donor ions in a region depleted of electrons. The donor concentration in the semiconductor is many orders of magnitude smaller than the electron concentration in the metal, so the uncompensated donors occupy a layer of appreciable thickness w and the bands in the semiconductor are bent upwards. The difference V_i between the electrostatic potentials outside the surfaces of the metal and semiconductor is given by $V_i = \delta\mathcal{E}_i$, where δ is their separation and $\mathcal{E}_i$ the field in the gap. If the metal and semiconductor approach each other, V_i must tend to zero if $\mathcal{E}_i$ is to remain finite. When the metal and the semiconductor finally touch as in figure 2.1(d), the barrier due to the vacuum disappears and we are left with an ideal metal-semiconductor contact. The quantity V_{d0} is the diffusion voltage at zero bias and the height of the barrier ϕ_b relative to the Fermi level is given by

$$\phi_b = \phi_m - \chi_s \tag{2.1}$$

The ideal situation of figure 2.1(d) is very seldom reached, because there is usually an interfacial layer of thin insulating oxide about 10-20 Å thick on the surface of the semiconductor. A practical contact is therefore more accurately described by figure 2.1(c); however, the barrier presented to the electrons by the oxide layer is usually so thin that electrons can easily tunnel through it and figures 2.1(c) and 2.1(d) are almost indistinguishable as far as the conduction electrons are concerned. Equation 2.1 is referred to as the Schottky-Mott limit.

In the model put forward by Schottky to explain the potential barrier, the semiconductor is assumed to be homogenous right up to the boundary with the metal, so that the uncompensated donors give rise to a uniform space charge in the depletion region. The electric field strength therefore increases linearly with distance from the edge of the depletion region to the metal surface in accordance with Gauss's theorem and the electrostatic potential increases quadratically. The resulting parabolic barrier is known as a Schottky barrier.

In practice it is found that equation 2.1 does not always give the correct barrier height. One of the reasons for this, apart from the presence of an interfacial layer, is the existence of localised surface states on the surface of the semiconductor. An explanation of the influence of surface states on the determination of the barrier height, was put forward by Bardeen (1947). A generalised analysis of the Bardeen model is also given in the book by Rhoderick *et al* (1988).

2.3 Current transport mechanisms

The various ways in which electrons can be transported across a metal-semiconductor junction under forward bias, are

a) emission of electrons from the semiconductor over the top of the barrier into the metal;
b) quantum-mechanical tunnelling through the barrier;
c) recombination in the space-charge region; and
d) recombination in the neutral region ("hole injection").

A Schottky Barrier Diode in which (a) is the most important, is referred to as "nearly ideal".

There are two basic mechanisms that govern the emission of electrons from the semiconductor over the top of the barrier into the metal. In the first process, electrons move from the bulk of the semiconductor and across the depletion region of the semiconductor by the mechanisms of drift and diffusion in the electric field of the barrier. At the interface, their emission into the metal is determined by the rate of transfer of electrons across the boundary between the metal and the semiconductor. These processes occur effectively in series. According to the diffusion theory, the first of these processes is the most important, whereas according to the thermionic-emission theory the second process is the limiting factor.

In the case of the Schottky barrier diodes used in this study, the thermionic-emission process was the limiting factor. According to this theory, provided the forward bias is not too large,

$$J = J_0 \exp(qV / nkT)[1 - \exp(-qV / kT)] \tag{2.2}$$

where J is the current density, n is the so-called ideality factor greater than unity and J_0 is given by

$$J_0 = A^{**}T^2 \exp\{-q(\phi_b - \Delta\phi_{bi}) / kT\} \tag{2.3}$$

where A^{**} is the Richardson constant and ϕ_b - $\Delta\phi_{bi}$ is the effective barrier height.

Of the other mechanisms of current transport in a semiconductor, only hole injection has further bearing on the work covered in this dissertation, and it will be covered in the next section.

2.4 Hole injection

If the height of a Schottky barrier on *n*-type material is greater than half the bandgap, as is often the case, the region of the semiconductor adjacent to the metal becomes *p*-type and contains a high density of holes. Some of these holes may diffuse into the neutral region of the semiconductor under forward bias, thus giving rise to the injection of holes.

Following the treatment of Scharfetter (1965) and Rhoderick *et al* (1988), if we assume that the hole quasi-Fermi level coincides with the Fermi level in the metal and remains flat throughout the depletion region, the hole current density can be written from ordinary p-n junction theory as

$$J_{\mathrm{h}} = \frac{qD_{\mathrm{p}}n_i^2}{LN_{\mathrm{d}}}[\exp(qV/kT) - 1] \tag{2.4}$$

where D_{p} and L are the diffusion constant of holes in the bulk semiconductor and the thickness of the neutral region, respectively. Assuming thermionic-emission theory, the electron current is given by equation 2.2 and the hole injection ratio γ_{h} is given by

$$\gamma_{\mathrm{h}} = \frac{J_{\mathrm{h}}}{J_{\mathrm{h}} + J_{\mathrm{e}}} \approx \frac{J_{\mathrm{h}}}{J_{\mathrm{e}}} = \frac{qD_{\mathrm{p}}n_i^2}{N_{\mathrm{d}}LA^{**}T^2\exp(-q\phi_b/kT)} \tag{2.5}$$

The above equation only takes into account the diffusion component of the hole current density and is adequate under low injection conditions. For sufficiently large forward bias, the electric field causes a significant carrier-drift current component that eventually dominates the minority carrier current. Under these conditions

$$\gamma_{\mathrm{h}} = \frac{n_i^2 J}{bN_{\mathrm{d}}^2 J_o} \tag{2.6}$$

where b is the ratio of the electron mobility to the hole mobility and for very large currents the injection ratio rises linearly with J.

Apart from the electrical technique of injecting holes by forward bias, these minority carriers can also be injected into the semiconductor by optical means. If the semiconductor is illuminated with light with an energy approximately equal to the bandgap, then electron-hole pairs are created. The electrons are swept away in the conduction band and the "injected" holes are then resident in the valence band.

The large current densities for which equation 2.6 is valid, are in the order of 350 A.cm^{-2}. In this work the value of J was 5.6 A.cm^{-2} and smaller, so equation 2.5 is taken as descriptive of the injection behaviour of the SBDs used.

Calculating the injection ratio at 125K using equation 2.5 and with $N_{\mathrm{d}} = 1.1 \times 10^{16}$ cm^{-3}, γ_{h} is of the order of 10^{-8}.

Chapter 3: Properties of Semiconductors

In this chapter a short overview is given of the important properties of semiconductors, with the emphasis on GaAs, that are necessary to understand the behaviour of simple devices manufactured on semiconductors. A more complete text can be found in for example (Sze 1981) and (Smith 1979).

3.1 Energy bands

The band structure of a crystalline solid, that is, the energy-momentum (*E-k*) relationship, is obtained by solving the Schrödinger equation of an approximate one-electron problem. The Bloch theorem states that if a potential energy $V(\mathbf{r})$ is periodic with the periodicity of the lattice, then the solutions $\phi_{\mathbf{k}}(\mathbf{r})$ of the Schrödinger equation

$$\left[-\frac{\hbar^2}{2m}\nabla^2 + V(\mathbf{r})\right]\phi_{\mathbf{k}}(\mathbf{r}) = E_{\mathbf{k}}\phi_{\mathbf{k}}(\mathbf{r}) \tag{3.1}$$

are of the form

$$\phi_{\mathbf{k}}(\mathbf{r}) = e^{j\mathbf{k}\cdot\mathbf{r}}U_n(\mathbf{k},\mathbf{r}) = \text{Bloch function} \tag{3.2}$$

where $U_n(\mathbf{k},\mathbf{r})$ is periodic in $\mathbf{r}$ with the periodicity of the direct lattice and n is the band index. From the Bloch theorem the energy $E_{\mathbf{k}}$ is periodic in the reciprocal lattice. For a given band index, to label the energy uniquely, it is sufficient to use only $\mathbf{k}$'s in a primitive cell in the reciprocal lattice.

The energy bands of semiconductors have been studied theoretically using principally three numerical methods, namely the orthogonalized plane-wave method (Allen 1955 and Herman 1955), the pseudopotential method (Phillips 1958) and the $\mathbf{k}\cdot\mathbf{p}$ method (Smith 1979). Figure 3.1 shows the energy-band structure for GaAs. Important is the forbidden energy region in which allowed states cannot exist. Energy bands are permitted above and below this energy gap. Above this gap they are called the conduction bands and below it they are called the valence bands. The separation between the energy of the lowest conduction band and the highest valence band is

called the bandgap E_g, which is the most important parameter of a semiconductor. Figure 3.2 is a simplified band diagram of a semiconductor.

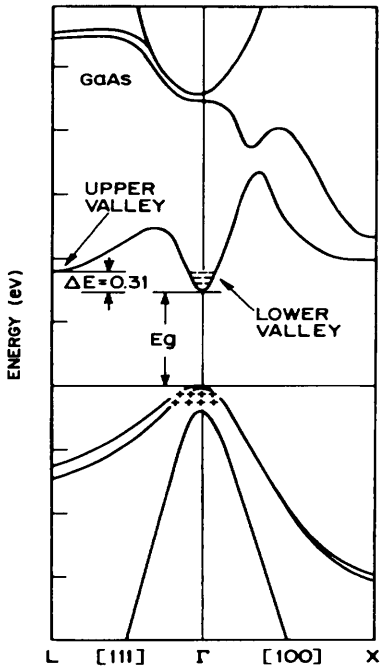

Figure 3.1: Energy band diagrams for GaAs, where E_g is the energy band bandgap. Plus signs indicate holes in the valence band and minus signs indicate electrons in the conduction band (Sze 1981).

At room temperature (300K) and under normal pressure, the bandgap of GaAs is 1.42 eV. Experimental results show that for GaAs the bandgap decreases with increasing temperature. The variation of bandgap with temperature is given by (Sze 1981)

$$E_g(T) = E_g(0) - \frac{\alpha T^2}{(T+\beta)} \tag{3.3}$$

where $E_g(0) = 1.519$ eV, $\alpha = 5.405 \times 10^{-4}$ eV K^{-1} and $\beta = 204$ K for GaAs.

3.2 Carrier concentration at thermal equilibrium

In figure 3.3, consider three basic bond pictures of a semiconductor. Silicon is used as an example for simplicity.

Figure 3.3(a) shows intrinsic silicon where each silicon atom shares its four valence electrons with the four neighbouring atoms, forming four covalent bonds. Figure 3.3(b) shows schematically *n*-type silicon, where a substitutional phosphorus atom with five valence electrons

has replaced a silicon atom and a negative-charged electron is "donated" to the conduction band. The silicon is *n*-type because of the addition of a negative charge carrier and the phosphorus atom is called a "donor". Figure 3.3(c) shows where a boron atom with three valence electrons substitutes for a silicon atom. An additional electron is "accepted" from the valence band to form four covalent bonds around the boron and a positive-charged "hole" is created in the valence band. This is *p*-type and the boron is an "acceptor". For *n*-type semiconductors the electron is referred to as the majority carrier and the hole as the minority carrier, since the electron concentration is the larger of the two. The roles are reversed for *p*-type semiconductors.

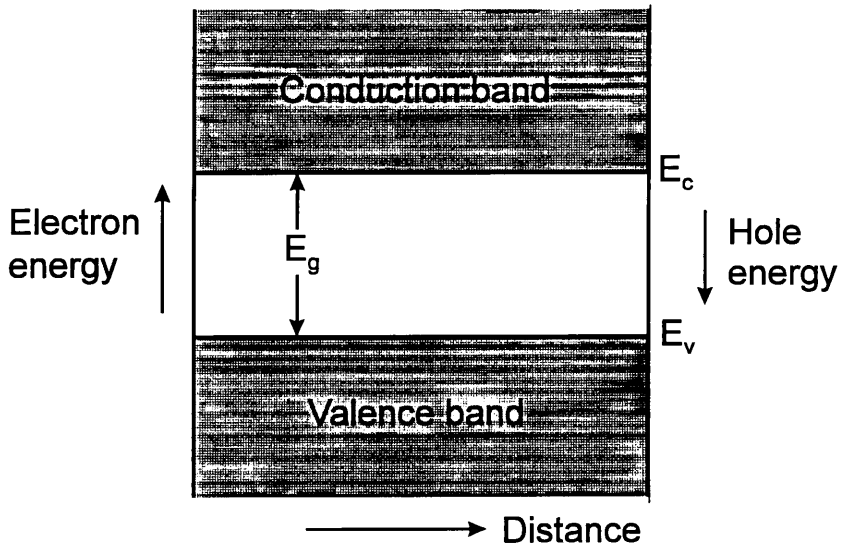

Figure 3.2: Simplified band diagram of a semiconductor.

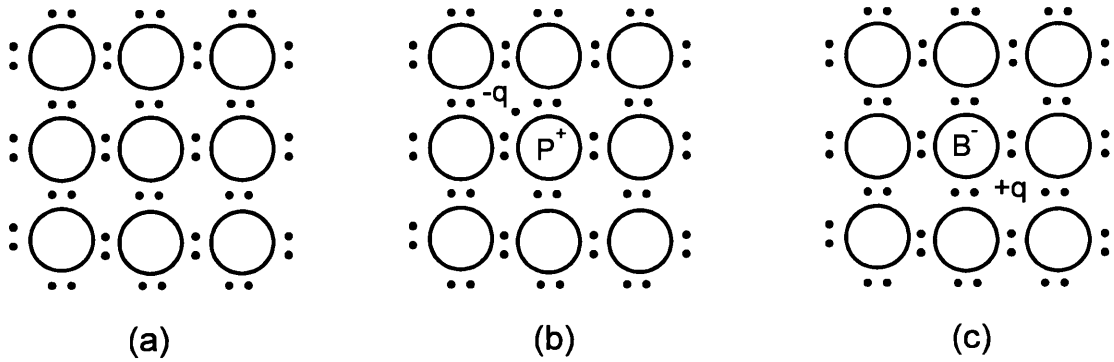

Figure 3.3: Three basic bond pictures of a semiconductor. (a) Intrinsic Si *with negligible impurities. (b)* n-*type* Si *with donor (phosphorus). (c)* p-*type* Si *with acceptor (boron).*

Consider now the case of the intrinsic semiconductor. The number of occupied conduction band levels is given by

$$n = \int_{E_C}^{E_{top}} N(E)F(E)dE \tag{3.4}$$

where E_C is the energy at the bottom of the conduction band and E_{top} is the energy at the top. The density of states $N(E)$ near the bottom of the conduction band for low-enough carrier densities and temperatures is

$$N(E) = M_c \frac{\sqrt{2}(E - E_c)^{1/2}}{\pi^2 \hbar^3} (m_{de})^{3/2} \tag{3.5}$$

where M_C is the number of equivalent minima in the conduction band and m_{de} is the density-of-state effective mass for electrons. The Fermi-Dirac distribution function $F(E)$ is given by

$$F(E) = \frac{1}{1 + \exp\left(\frac{E - E_F}{kT}\right)} \tag{3.6}$$

where k is Boltzmann's constant, T the absolute temperature and E_F the Fermi energy. Equation 3.4 can then be evaluated to be

$$n = N_c \frac{2}{\sqrt{\pi}} F_{1/2}\left(\frac{E_F - E_C}{kT}\right) \tag{3.7}$$

where N_C is the effective density of states in the conduction band and is given by

$$N_C \equiv 2\left(\frac{2\pi m_{de} kT}{h^2}\right)^{3/2} M_C \tag{3.8}$$

and $F_{1/2}(\eta_f)$ is the Fermi-Dirac integral. For the Boltzmann statistics case, i.e. for the Fermi level several kT below E_C in nondegenerate semiconductors, the integral approaches $\sqrt{\pi}\, e^{\eta_f} / 2$ and equation 3.7 becomes

$$n = N_C \exp\left(-\frac{E_C - E_F}{kT}\right). \tag{3.9}$$

Similarly, the hole density near the top of the valence band is

$$p = N_V \frac{2}{\sqrt{\pi}} F_{1/2}\left(\frac{E_V - E_F}{kT}\right) \tag{3.10}$$

where N_V is the effective density of states in the valence band and is given by

$$N_V = 2\left(\frac{2\pi m_{dh} kT}{h^2}\right)^{3/2} \tag{3.11}$$

where m_{dh} is the density-of-state effective mass of the valence band. Again under nondegenerate conditions it follows that

$$p = N_V \exp\left(-\frac{E_F - E_V}{kT}\right). \tag{3.12}$$

For intrinsic semiconductors at finite temperatures continuous thermal agitation exists, which results in electrons being excited from the valence band to the conduction band and leaves an equal number of holes in the valence band. Thus $n = p = n_i$, where n_i is the intrinsic carrier density. This process is balanced by recombination of the electrons in the conduction band with holes in the valence band.

The Fermi level for an intrinsic semiconductor is obtained by equating equations 3.9 and 3.12:

$$E_F = E_i = \frac{E_C + E_V}{2} + \frac{3kT}{4}\ln\left(\frac{m_{dh}}{m_{de}M_c^{2/3}}\right). \tag{3.13}$$

From this it can be seen that the Fermi level E_i of an intrinsic semiconductor generally lies very close to the middle of the bandgap.

The intrinsic carrier density follows from equations 3.9, 3.12 and 3.13:

$$np = n_i^2 = N_C N_V \exp(-E_g / kT) \tag{3.14}$$

or

$$n_i = 4.9 \times 10^{15}\left(\frac{m_{de}m_{dh}}{m_0^2}\right)^{3/4} M_c^{1/2} T^{3/2} e^{-E_g/2kT} \tag{3.15}$$

Thus, the larger the bandgap is, the smaller the intrinsic carrier density will be.

When a semiconductor is doped with donor or acceptor impurities, impurity energy levels are introduced in the forbidden bandgap. A donor level is defined as being neutral if filled by an electron and positive if empty. An acceptor level is neutral if empty and negative if filled by an electron. The simplest calculation of impurity energy levels is based on the hydrogen-atom model. This simple model cannot account for the details of ionisation energy, particularly for deep levels in semiconductors, but it does predict the correct order of magnitude of the true ionisation energies for shallow impurities.

As was seen in equation 3.13, the Fermi level for the intrinsic semiconductor lies very close to the middle of the bandgap. When impurity atoms are introduced, the Fermi level must adjust itself to preserve charge neutrality. Consider the case of donor impurities, concentration N_D. The

total negative charges (electrons and ionised acceptors) must equal the total positive charge (holes and ionised donors) to preserve charge neutrality. In the case of donor impurities

$$n = N_D^+ + p \tag{3.16}$$

where n is the electron density in the conduction band, p the hole density in the valence band and N_D^+ is the number of ionised donors

$$N_D^+ = N_D\left[1 - \frac{1}{1 + \frac{1}{g}\exp\left(\frac{E_D - E_F}{kT}\right)}\right] \tag{3.17}$$

where g is the ground state degeneracy of the donor impurity level and equals 2 for GaAs (figure 3.1) because of the fact that a donor level can accept one electron with either spin or can have no electron. In the case of acceptor impurities of concentration N_A, the expression for ionised acceptors is

$$N_A^- = \frac{N_A}{1 + g\exp\left(\frac{E_A - E_F}{kT}\right)} \tag{3.18}$$

where the ground-state degeneracy factor g is 4 for acceptor levels as a result of the two degenerate valence bands at $\mathbf{k} = 0$ (see figure 3.1).

For a set of given N_C, N_D, N_V, E_c, E_D, E_V and T the Fermi level can be uniquely determined using equations 3.9, 3.12, 3.16 and 3.17. As the temperature is lowered sufficiently, the Fermi level rises toward the donor level (for n-type semiconductors) and the donor level is partially filled with electrons.

When impurity atoms are added, the np product is still given by equation 3.14 and the product is independent of the added impurities. At relatively elevated temperatures, most donors and acceptors are ionised, e.g. Si, which lies 0.0058 eV below the conduction band at 300 K, so the neutrality condition can be approximated by

$$n + N_A = p + N_D \tag{3.19}$$

Equations 3.14 and 3.19 can be combined to give the concentration of electrons and holes in an n-type semiconductor:

$$\begin{aligned} n_{no} &= \tfrac{1}{2}\left[(N_D - N_A) + \sqrt{(N_D - N_A)^2 + 4n_i^2}\right] \\ &\approx N_D \text{ if } |N_D - N_A| >> n_i \text{ and } N_D >> N_A \end{aligned} \tag{3.20}$$

$$p_{no} = n_i^2 / n_{no} \cong n_i^2 / N_D \tag{3.21}$$

and

$$E_C - E_F = kT \ln\left(\frac{N_C}{N_D}\right) \tag{3.22}$$

or from equation 3.13

$$E_F - E_i = kT \ln\left(\frac{n_{no}}{n_i}\right) \tag{3.23}$$

The expressions for *p*-type semiconductors follow similarly.

3.3 Carrier transport phenomena

There are several phenomena that play a role in the transport of carriers in a semiconductor, namely mobility, resistivity and recombination processes. Mobility and resistivity are defined and described in any good semiconductor handbook, e.g. Smith (1979) or Sze (1981). Recombination processes have more bearing on the work reported on in this dissertation and will be discussed in more detail.

Recombination processes come in several different guises. In band-to-band recombination, an electron-hole pair recombines. The transition of an electron from the conduction band to the valence band is made possible by the emission of a photon (radiative process) or by transfer of the energy to another free electron or hole (Auger process).

In single level recombination of electrons and holes, only one trapping energy level (E_T) is present in the bandgap, i.e. the trapping level lies between E_C and E_V in figure 3.2. The recombination takes place via this trapping level and is typically found in semiconductors where irradiation has introduced defect levels in the bandgap. The single level recombination can be described by four processes: electron capture, electron emission, hole capture and hole emission. They are illustrated schematically in figure 3.4.

Which of these electronic transitions dominates, is determined by the respective emission and recombination rates. These rates depend on the free energy of ionisation, the capture cross-sections for electrons and holes of the defect level and the temperature.

In the following, the formalism introduced by Shockley *et al* (1952) is followed:

To illustrate the basic mechanisms at work, consider an electron trap in a *n*-type semiconductor. The mechanisms are governed by Fermi-Dirac statistics. The probability that a quantum state will be occupied in thermal equilibrium, is given by

$$f(E_T) = \frac{1}{1 + \exp[(E_T - E_F)/kT]} \tag{3.24}$$

where E_T is the trap energy, E_F is the Fermi level, k is Boltzmann's constant and T is the temperature. The probability that the state is empty, is given by $f_p = 1 - f$.

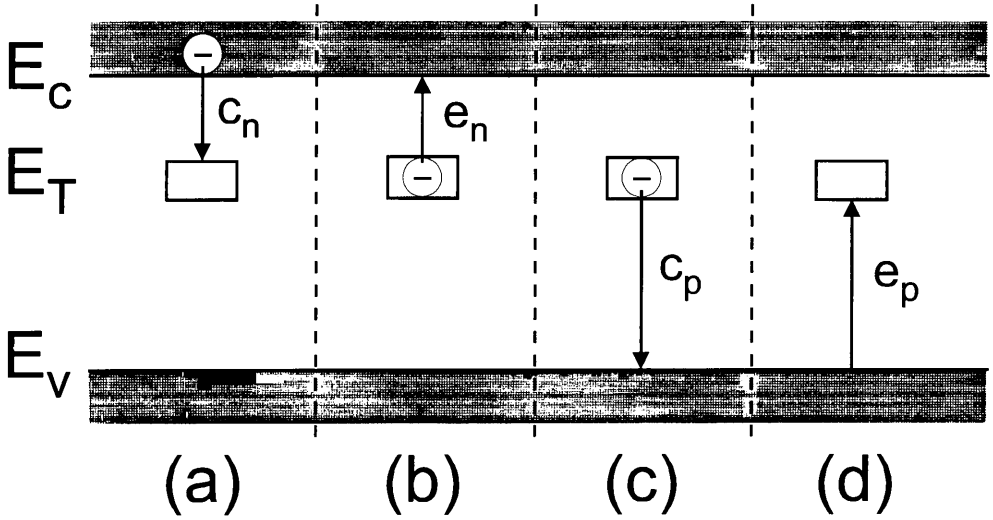

Figure 3.4: The basic processes involved in recombination by trapping: (a) electron capture, (b) electron emission, (c) hole capture, (d) hole emission. The constants c *and* e *refer to capture and emission respectively and the subscripts* n *and* p *refer to electrons and holes respectively.*

The capture rate is governed by three factors: the number of empty traps that can capture an electron, given by $f_{pT}N_T$, the number of states in the conduction band that are occupied by an electron, given by $f(E)N(E)dE$, and the average probability per unit time that the empty trap will capture an electron with energy in the range dE, given by $c_n(E)$. Here N_T is the number of traps per unit volume and $N(E)$ is the density of energy levels in the conduction band.

The capture rate is then given by

$$dU_c = f_{pT}N_T c_n(E) f(E) N(E) dE \tag{3.25}$$

where the capture constant

$$c_n(E) = \nu_{th}\sigma_n \tag{3.26}$$

and σ_n is the capture cross-section of the trap for electrons.

The same logic is applied to calculate the emission rate:

$$dU_e = (f_T N_T)(e_n(E))(f_p(E)N(E)dE) \tag{3.27}$$

where $e_n(E)$ is the emission constant.

At thermal equilibrium, the net capture rate is given by

$$dU_{ce} = dU_c - dU_e = \left[f_{pT} f(E) - \frac{e_n}{c_n} f_T f_p(E)\right] M_n(E) N_T N(E) dE \tag{3.28}$$

For thermal equilibrium, the expression in the square brackets equals zero, giving

$$\frac{e_n}{c_n} = \exp\left(\frac{E_T - E}{kT}\right) \tag{3.29}$$

In the case of non-degenerate statistics, the probability that a state will be empty (f_p) is nearly unity for the states in the conduction band, and consequently the emission constant e_n is only a function of the fraction of traps occupied by electrons (f_t) [Schockley *et al*, 1952].

The recombination rate U in $cm^{-3}.s^{-1}$ is given by [Sze 1981]

$$U = \frac{\sigma_p \sigma_n \upsilon_{th} (pn - n_i^2) N_T}{\sigma_n \left[n + n_i \exp\left(\frac{E_T - E_i}{kT}\right)\right] + \sigma_p \left[p + n_i \exp\left(-\frac{E_T - E_i}{kT}\right)\right]} \tag{3.24}$$

where σ_p and σ_n are the hole and electron capture cross sections, ν_{th} the thermal velocity, N_T the trap density, E_T the trap energy level, E_i the intrinsic Fermi level and n_i the intrinsic carrier density. In thermal equilibrium $pn = n_i^2$ and thus $U = 0$. Furthermore, under the simplification that $\sigma_n = \sigma_p = \sigma$, equation 3.24 reduces to

$$U = \sigma \upsilon_{th} N_T \frac{pn - n_i^2}{n + p + 2n_i \cosh\left(\frac{E_T - E_i}{kT}\right)} \tag{3.25}$$

The recombination rate approaches a maximum as the energy level of the recombination centre approaches midgap ($E_T \approx E_i$). Thus the most effective recombination centres are those located near the middle of the bandgap. The energy levels close to the middle of the bandgap that are efficient recombination centres can come from impurities in the semiconductor, e.g. gold in silicon and from particle irradiation of the semiconductor, which causes displacement of host atoms and lattice damage that leads to the introduction of energy levels in the bandgap. An example is electron irradiation of Si that leads to a donor level 0.36 eV below the conduction band.

For multiple-level traps the recombination processes have gross qualitative features that are similar to the single-level case.

Chapter 4: Deep Level Transient Spectroscopy

The study of electrical properties of semiconductors by means of transient capacitance methods is a well established technique in experimental physics. The specific technique used in this study to observe the electrical properties of defects, was the so-called Deep Level Transient Spectroscopy (DLTS) method, pioneered by D.V. Lang in 1974 [Lang 1974; Miller *et al.*1977]. The scope of this chapter is to give a brief background to the DLTS method and to show how it leads to the determination of the properties of a deep level defect.

4.1 The properties of a semiconductor junction

In the case of a semiconductor junction, the application of a reverse bias creates a depletion layer that lies almost entirely in the lightly doped material. The width W of this depletion (or "space-charge") layer is given by

$$W = \sqrt{\frac{2\varepsilon(V_{bi} + V)}{qN}} \tag{4.1}$$

where ε is the dielectric constant of the depleted semiconductor material, V_{bi} is the built-in bias voltage of the junction, V is the externally applied bias voltage, q is the charge on the electron and N is the density of ionised doping centres in the lightly doped material. This equation indicates that W increases roughly as $\sqrt{V}$ and depends on the doping and dielectric constants of the underlying semiconductor material. It is also clear that the reverse-biased structure essentially forms a parallel plate capacitor, comprising a layer of dielectric of thickness W and dielectric constant ε between two conducting electrodes. The capacitance of this capacitor decreases monotonically with increasing bias voltage.

In this picture of a reverse-biased semiconductor junction, the back edge of the depletion layer is that region where the electric field is zero, since at that location the electric field created by the applied bias voltage is exactly balanced by the electric field due to all of the exposed ionised dopant centres within the depletion layer. Thus if the reverse bias voltage is increased from V to

$V+\Delta V$, then the depletion layer width W must expand by an amount ΔW sufficient to uncover enough additional charge ΔQ per unit area to cancel out the electric field increment ΔE

$$\Delta E = \frac{\Delta V}{W} = \frac{\Delta Q}{\varepsilon} = \frac{qN(W)\Delta W}{\varepsilon} \tag{4.2}$$

Here $N(W)$ is the local doping density at the back edge of the depletion layer. This equation, in conjunction with the equation

$$C = \frac{\varepsilon A}{W} \tag{4.3}$$

can be made the basis of "junction-profiling" measurements that display $N(W)$ versus W for abrupt junctions. The spatial resolution of this electrical junction profiling is limited by the local Debye length l_D, given by

$$l_D = \sqrt{\frac{kT\varepsilon}{q^2 n}} \tag{4.4}$$

where k is Boltzmann's constant, T is the absolute temperature and n is the free carrier density at the location of interest.

4.2 Defect states in the bandgap

For the purposes of this discussion, a defect state may be defined as an electronic energy state introduced into the forbidden gap of a semiconductor as a result of a perturbation of the bonding structure of the host material by the presence of a lattice defect or impurity. A distinction is made between **shallow states**, which are located near their related band edges, i.e. the valence band for acceptors and the conduction band for donors, with the associated ionisation energy approximately described by a modified hydrogenic model, and **deep states**, which are positioned deeper than the corresponding hydrogenic states and thus have large ionisation energies. As a result of the localised nature of a deep state in the semiconductor lattice, carrier capture or emission on the deep state is often accompanied by lattice relaxation phenomena as the defect bonds adjust to local carrier interactions.

In a neutral semiconducting material, a deep defect state is defined as an electron trap if the electron capture rate c_n is much larger than the hole capture rate c_p, and defined as a recombination centre if both the electron and hole capture rates are large, i.e. $c_n \sim c_p$. The electron and hole capture rates are given by the respective expressions

$$c_n = \sigma_n \langle \upsilon_n \rangle n \tag{4.5}$$

and

$$c_p = \sigma_p \langle \upsilon_p \rangle p \tag{4.6}$$

where n and p are the concentration of electrons and holes, σ_n and σ_p the electron and hole capture cross sections and $\langle \upsilon_n \rangle$ is the average thermal velocity of electrons given by

$$\langle \upsilon_n \rangle \cong \sqrt{\langle \upsilon_n^2 \rangle} = \sqrt{\frac{3kT}{m_e^*}} \tag{4.7}$$

where m_e^* is electron effective mass, k is Boltzmann's constant and T is the absolute temperature. An analogous expression holds for holes.

Now, in the depletion layer of a reverse-biased semiconductor junction, two classes of defects are defined in terms of their thermal emission properties, namely majority and minority carrier traps. A majority carrier trap is defined as a defect where the rate for thermal emission of a majority carrier e_{maj} is much larger than the corresponding rate for thermal emission of a minority carrier e_{min} . For a minority carrier trap $e_{min} >> e_{maj}$. In the context of capacitance spectroscopy, a majority carrier trap is a defect which may be somehow induced to capture a majority carrier and is then subsequently observed by the effect which emitting this carrier has on the junction capacitance.

Thermal emission rates are proportional to a Boltzmann factor exp(-$\Delta E/kT$), where ΔE is the depth of the trap from the band edge to which the carrier is emitted. Thus, for electron emission and using the principle of detailed balance,

$$e_n = \frac{\sigma_n \langle \upsilon_n \rangle N_c}{g} \exp(-\Delta E / kT) \tag{4.8}$$

where $\Delta E = E_C - E_T$, with E_C and E_T the conduction band and defect state energies respectively, T is the absolute temperature, k is Boltzmann's constant, N_C is the effective density of states at the conduction band edge and g is the degeneracy of the level. An analogous expression holds for hole emission with the subscripts n replaced by p, N_C replaced by N_V and $\Delta E = E_T - E_V$.

Now that the emission rate is defined, the rate equations governing the occupation of a defect state are introduced. In the following, quantities with a superscript "o" denote "optical", e.g. e_n^o is the optical electron emission rate. For a defect state of total concentration N_T, the rate equations are

$$\frac{dN}{dt} = (c_n + e_p + e_p^o)(N_T - N) - (c_p + e_n + e_n^o)N \tag{4.9}$$

where N is the concentration of defects occupied by electrons. Important to note are the exponential time dependence of solutions to equation 4.9 and that the time constant of this exponential is the sum of all the rates of carrier capture and emission for the defect. In thermal capture and emission only one of the six rates usually dominates so that the solutions are considerably simplified, e.g. the electron capture process into an initially empty electron trap is given by

$$N(t) = N_T(1 - e^{-c_n t}) \tag{4.10}$$

where all rates except c_n are set to zero. The emission process following the capture of this electron in the depletion layer is given by

$$N(t) = N_T\, e^{-e_n t} \tag{4.11}$$

where all rates except e_n are set to zero.

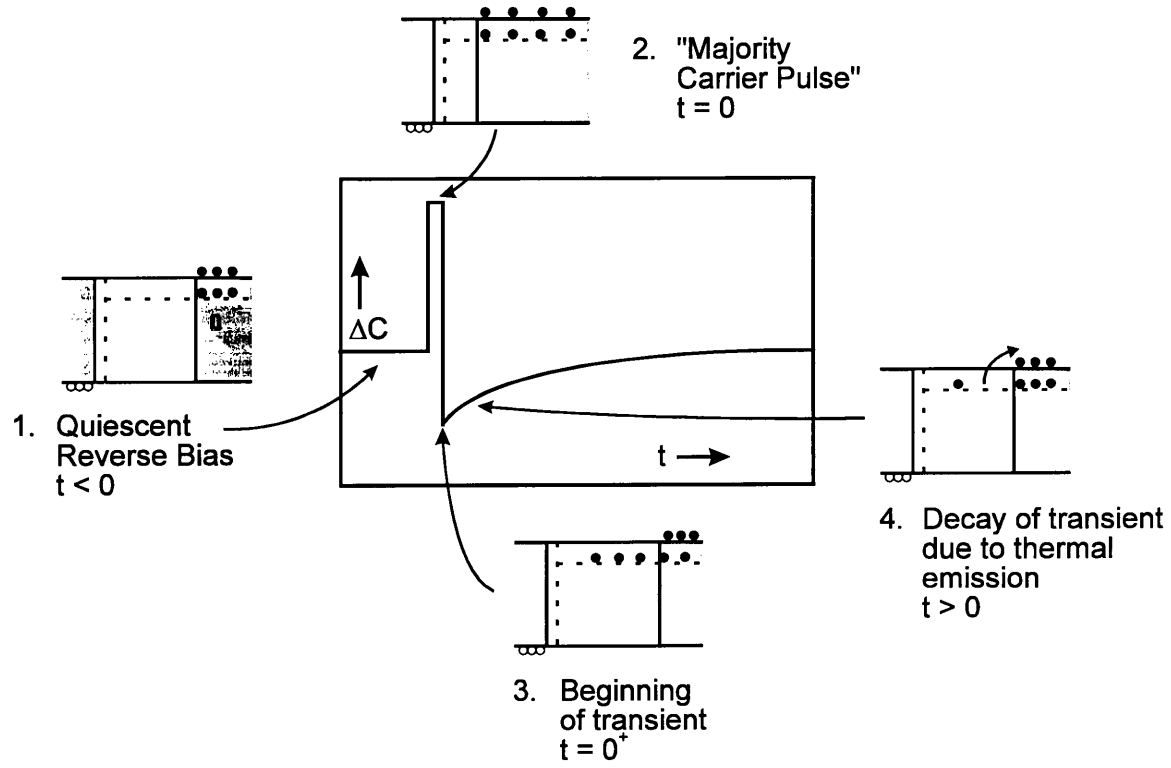

Figure 4.1: Capacitance transient due to a majority carrier trap in a p^+-n diode. The small schematics show the charge state of the defect level and the width of the space charge region (unshaded) at various times before and during the transient.

4.3 The effect of deep level defect states on junction capacitance transients

In the space charge region of a reverse-biased semiconductor junction, electronic transitions consist entirely of emission processes, since no carriers are available for capture; thus junction capacitance response may be interpreted solely in terms of emission rates (equation 4.8). Since states within the space charge region have no possibility of being filled by capture processes, emission processes can only be observed following the forced introduction of carriers which are to be captured. This is accomplished by pulsing the junction bias. Figure 4.1 illustrates this pulsing sequence schematically and also shows the accompanying capacitance transients that result from the emission processes.

Initially the junction is under reverse bias V_r to establish space charge dominant conditions. States in the space charge region are empty, since no carriers are available for capture. A bias pulse V_p towards zero superimposed on V_r will momentarily collapse the space charge region, making majority carriers available for capture. When V_r is re-established, the junction capacitance is reduced from the value before the pulse because compensating majority carrier charge has been trapped in the space charge region (refer equations 4.1 and 4.3). This charge can subsequently be excited in a bound-to-band transition by thermal emission and swept from the space charge region by the potential V_r. Since the emission processes are exponential, the capacitance transient shows exponential decay. The characteristic decay time constant (τ) of this transient is related to the emission rate e_n by

$$e_n = 1/\tau \tag{4.12}$$

Each defect state may be studied independently through its unique activation energy for carrier emission and its cross section for carrier capture.

4.4 Determination of defect state parameters from capacitance transients

The defect parameters obtainable via capacitance transient spectroscopy are the defect energy level, capture cross section and defect concentration.

From equation 4.8, the slope of an Arrhenius plot of ln e_n versus $1/T$ yields the activation energy for carrier emission, but there is the complication of the temperature dependence of the prefactor in equation 4.8. The T^2 dependence of the product $\langle \upsilon_n \rangle N_c$ is usually taken into account by constructing an Arrhenius plot of ln $e_n T^{-2}$ versus $1/T$, with the temperature dependence of the capture cross section neglected. In this vein, it is also noted here that the energy determination is

complicated by the electric field dependence of the thermal emission rate and the fact that ΔE in equation 4.8 is a free energy, whereas the thermodynamic quantity derived from the temperature dependence of the emission rate is an enthalpy. In practice these complications are neglected and the energy derived from the plot of ln $e_n T^{-2}$ vs $1/T$ is taken as the defect energy level.

The capture of carriers normally proceeds exponentially during an injection or zero bias pulse according to equation 4.10 if $\Delta C << C$. The capture rate is obtained by measuring the capacitance signal following the pulse as a function of pulse duration and then extracting the capture rate from the slope of ln $[C_\infty - C(\tau)]$ versus τ, where τ is the duration of the pulse. For majority carrier capture, the capture cross section is then obtained from equation 4.5 or 4.6.

The capture cross section can also be obtained from the prefactor of equation 4.8. However, this method often gives a different answer to the zero bias pulse method outlined above. The differences are often ascribed to the large temperature dependencies of some capture cross sections and the influence of the sometimes large electric fields present in the depletion region. For this reason the capture cross section obtained from the prefactor of equation 4.8 is often referred to as the apparent capture cross section.

Considering the measurement of defect concentration, if $\Delta C << C$ and the doping is spatially uniform, we have, in n-type material, (Miller *et al* 1977)

$$N_T \cong 2(N_D - N_A)\frac{\Delta C}{C} \tag{4.12}$$

where ΔC is the capacitance change due to completely filling a trap of concentration N_T in the depletion layer and C is the capacitance of that depletion layer. This expression is actually quite inaccurate, since the pulse used to fill the traps does not cover the entire depletion layer. More accurately we have (Miller *et al* 1977)

$$\delta\left(\frac{\Delta C}{C}\right) = \left(\frac{\varepsilon}{qW^2 N^+}\right)\frac{N_T(x)}{N^+(x)}\delta V \tag{4.13}$$

where $\delta(\Delta C/C)$ is the incremental change in the relative capacitance signal due to the traps filled by the small change δV in the reduced-bias pulse of amplitude V corresponding to a depletion layer width of x during the pulse. The quantities C, W and N^+ are the capacitance, depletion layer width and ionised shallow level concentration at the edge of the depletion layer for the applied reverse bias. In this way the uniformity of defect concentrations and arbitrary defect profiles may be determined.

4.5 Important principles of DLTS

The main feature of DLTS as an experimental measurement technique, is that it is a transient capacitance method. In the DLTS method, the time constant of the decaying output signal is displayed using the so-called "rate window".

If the capacitance-versus-time information from a transient capacitance experiment is processed so that a selected decay rate produces a maximum output, then a signal whose decay time constant changes monotonically with time reaches a peak when the rate passes through the rate window. Thus observing a semiconductor junction repetitive capacitance transient while slowly scanning the sample temperature results in the appearance of a peak in the temperature versus output plot. Such a plot is called a DLTS spectrum.

The rate window was originally implemented by a double boxcar integrator. In this study the rate window was implemented using a lock-in amplifier-based system, which is described in detail by Goodman (1994).

Chapter 5: Defects in GaAs

Defects in the crystal structure of semiconductors exist in the bulk material, at the surface and interfaces and originate from the material itself, e.g. grown in during material growth, or they are produced during the various steps involved in the processing of semiconductor devices. Defects play a major role in the determination of the electronic properties of a semiconductor, mainly because they interact with free carriers in the form of traps, recombination centres and scattering centres. Their effect is of importance even when their concentration is very small compared to the free carrier concentration.

In this chapter the focus will be on defects in GaAs, with a short summary of point defects, a phenomenological view of the effects of irradiation on GaAs and a short discussion on the properties of metastable defects. Point defects in GaAs are extensively discussed by Bourgoin *et al* (1986), while the effects of irradiation are reviewed by Lang (1977) and Pons *et al* (1985). The reader is also referred to the excellent books on Point Defects in Semiconductors by Lannoo *et al* (1981) and Bourgoin *et al* (1983).

5.1 Point defects

A point defect in a crystal is an entity that causes an interruption in the lattice periodicity. This can happen in the following number of ways:

a) An atom is removed from its regular lattice site - this defect is called a vacancy.
b) An atom is in a site different from a regular lattice site - this defect is called an interstitial. If the interstitial defect is of the same species as the lattice, it is an intrinsic defect and when it is of a different species than the lattice, it is an extrinsic defect (interstitial impurity).
c) An impurity occupies a substitutional site.

In the case of GaAs, there are two different sublattices, each having its own vacancy, its own interstitial and its own substitutional impurities. The nomenclature is as follows: As and Ga vacancies are indicated by V_{As} and V_{Ga} and interstitials by As_i and Ga_i. An atom of one sublattice placed in the other sublattice forms an antisite defect and are indicated by As_{Ga}, i.e. an arsenic

atom in a gallium lattice position and Ga_{As}, which in turns indicates a gallium atom in an arsenic lattice position.

Various kinds of defects are also formed by the association of above mentioned defects with each other and with impurities in the lattice. In such a way a Frenkel pair is a close vacancy-interstitial pair (e.g. V_{As}-As_i), two neighbouring vacancies form a divacancy, etc. Small aggregates of point defects, like those just mentioned, are considered to still be point defects.

5.2 Complex defects

When a simple defect, i.e. a point defect, moves, it can interact with other intrinsic and extrinsic defects giving rise to a more complex defect, e.g. in GaAs the mobile arsenic interstitial As_i can form the complexes As_i-B with boron and As_i-C with carbon. When the concentration of a particular defect is large, they tend to aggregate as the temperature is increased, so that for example vacancies will form trivacancies and quadrivacancies and extrinsic defects will aggregate to form clusters of impurity defects.

5.3 Lattice distortion and relaxation

The introduction of a point defect induces displacements of the lattice atoms which surround it. The atoms involved are first neighbours, second neighbours and so on in the crystal lattice. The range over which the displacement is felt, depends on the specific point defect. When the symmetry of the lattice is conserved, these displacements are said to result in a relaxation of the lattice. When the symmetry is lowered, the displacements are said to result in a distortion. Since a defect perturbs the periodicity of the perfect lattice, its presence can introduce electronic states in the forbidden bandgap of the semiconductor. It is the study of these levels in the bandgap that is the gateway to understanding the properties and structure of the defects themselves. This is especially true for GaAs, since techniques like electron paramagnetic resonance (EPR) have so far been difficult to implement due to the large hyperfine line broadening in III-V compounds.

5.4 Effect of irradiation on GaAs

Various types of irradiation have been used to study the properties of semiconductors through the defects that the irradiation induce in the crystal structure of the semiconductor. Electron irradiation, proton and neutron particle irradiation and ion implantation have been used, of which electron irradiation has been the most widely used.

In the case of electron irradiation, for electron energies in the range 0.25 - 1.0 MeV, the electron can only transfer enough energy to displace a single lattice atom. This irradiation creates simple point defects. A typical DLTS spectrum of electron irradiated n-GaAs is shown in figure 5.1.

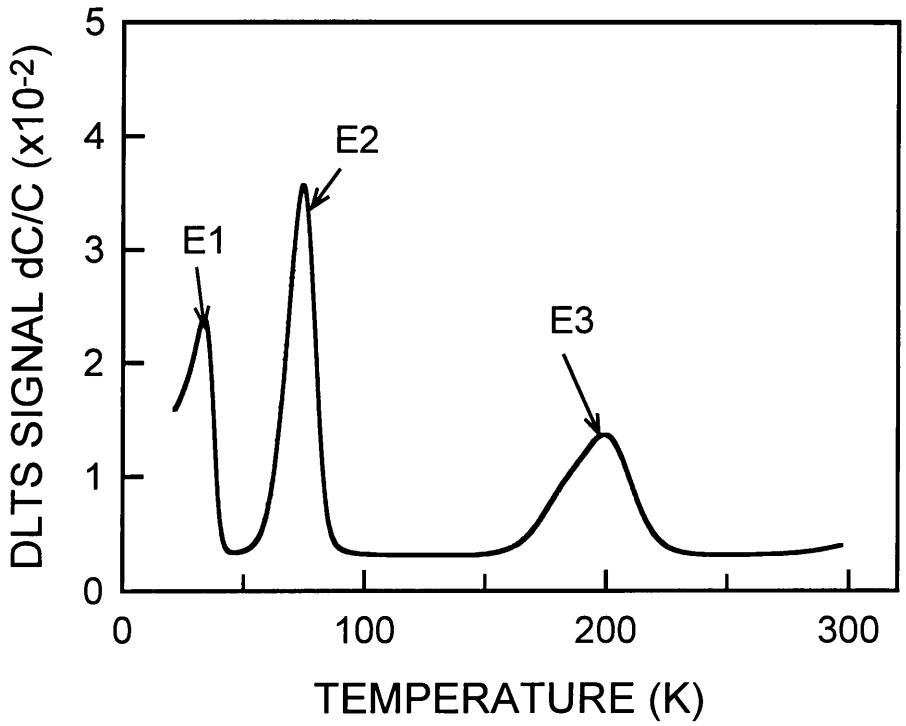

Figure 5.1: A DLTS spectrum of Si-doped n-GaAs, carrier concentration 1×10^{16} cm^{-3}, *irradiated with electrons from a* ^{90}Sr *radionuclide source (Auret* et al *1993b) showing the characteristic defect peaks E1, E2 and E3 of electron irradiation.*

The defects identified as E1-E3 are characteristic of electron irradiation and are associated with vacancy-interstitial pairs in the As sublattice (Pons *et al* 1985). As the electron energy increases, enough energy is transferred to the primary knock-on atom to displace a second and third atom from their lattice sites in a cascade, thus creating a higher concentration of defects. The number of displacements produced by a single primary collision can thus be very high.

For proton and neutron irradiated n-GaAs, the DLTS spectra show the same main features as the electron irradiated samples, namely the peaks E1, E2 and E3, although in different concentrations. This is to be expected, since protons and neutrons create much more damage in the crystal structure; either closely spaced point defects which mutually perturb each other's energy levels or extended defects where point defects lose their identity. The same argument

applies to ion implantation and in the case of this study, the ions under consideration are He nuclei or α-particles. A DLTS spectrum of α-particle irradiated n-GaAs is shown in figure 5.2.

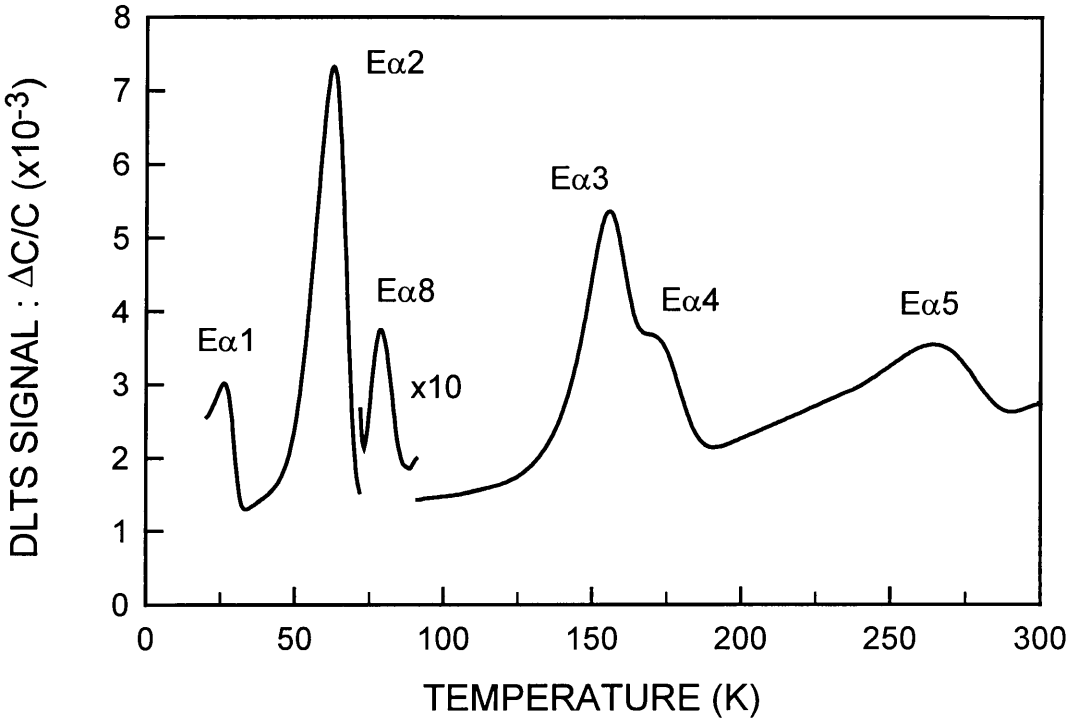

Figure 5.2: A DLTS spectrum of Si-doped n-GaAs, carrier concentration 1×10^{16} cm^{-3}, *irradiated with α-particles from an* ^{241}Am *radionuclide source, showing the defect peaks Eα1-Eα5 and Eα8 introduced by α-particle irradiation. The electronic properties of these defects have been reported by Auret* et al *(1993b) and Goodman* et al *(1993) and it was shown that the defects Eα1, Eα2 and Eα4 have the same DLTS signatures as the well-known electron irradiation induced defects E1, E2 and E3, respectively.*

Each defect level in the forbidden bandgap has certain unique parameters that characterise it. In the case of an electron trap, the energy level E_T of the defect below the conduction band and the defect capture cross section $\sigma(T)$ for capture of electrons constitute the so-called "defect signature". This defect signature in conjunction with the annealing kinetics and field enhanced emission properties can be used to identify the defect unambiguously once a certain signature has been linked to a certain defect configuration. The chapter on deep level transient spectroscopy will deal with the procedures to determine E_T and $\sigma(T)$.

5.5 Metastable defects

As described by Watkins (1989), in a crystalline solid the arrangement of atoms is usually associated with a periodic potential that describes the interactions of the atoms and their associated electron clouds. "Configurational space" is then a representation of the energy surfaces in a crystal as we move from one atom to the next. When we consider a defect in a crystal, which as mentioned perturbs the periodicity of the lattice, we can expect more than one local minimum in the configurational space in the vicinity of the defect. Only one of these minima - the lowest in energy - will be the stable configuration and the one that is normally encountered. The other local minimum or minima will be metastable. If, however, the energy barriers and energy differences between the stable configuration and one or more of the metastable configurations are not too large, it is possible to excite the defect into one or more of its metastable configurations, for example by changing the charge state of the defect, by carrier injection or by optical excitation with the correct energy.

Such a system, where the metastable configurations are accessible by excitation, is conveniently discussed in terms of a "configurational coordinate" (C-C) diagram, where the total energy of the system is plotted vs. a single generalised distortion coordinate Q which serves to describe the combined atomic rearrangements as one passes on a minimum energy path from one local minimum to another in configuration space. In figure 5.3 we show a set of diagrams for a defect which in charge state n has a stable lattice configuration A and a metastable one labelled B with a barrier between them.

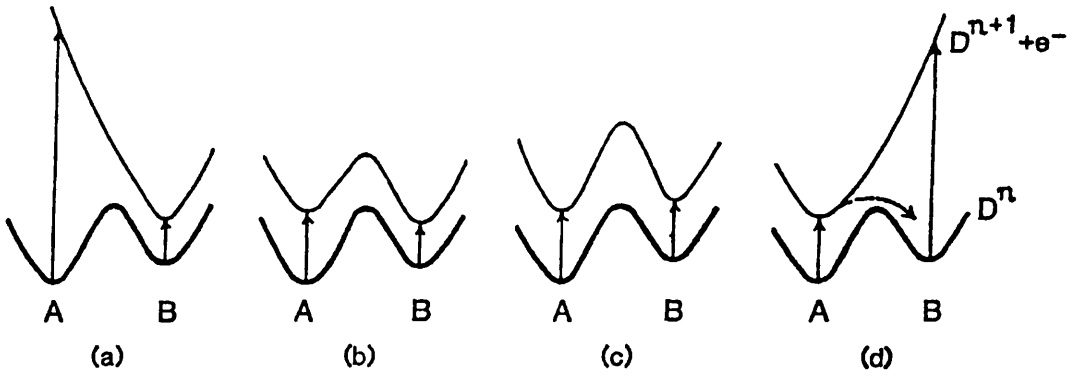

Figure 5.3: Four possible C-C diagrams for a metastable defect with two lattice configurations.

The four diagrams differ only in the properties of the excited ionised state $D^{n+1} + e^-$, representing the four commonly occurring possibilities. In the case of figure 5.3 (a) and (d), the excited state has a local minimum only in either configuration B or A, respectively. These cases are often referred to as large lattice relaxation cases because large Stokes shifts are present, the vertical optical ionisation energy being much larger than the true ionisation energy. In the case of figure 5.3 (b) and (c), the excited states display both local minima, but they differ as to whether configuration A or B has the lowest minimum. These are referred to as small lattice relaxation cases because large Stokes shifts are absent.

In the case of figure 5.3 (a) and (b), the stable configuration is different for the D^n and D^{n+1} charge states. The defect is then said to be bistable and can be converted from one configuration to the other simply by changing its charge state at a temperature where the energy barriers are surmountable. Cooled to below this temperature, the defect is frozen into a specific configuration and its electrical and optical properties can be measured directly. Junction capacitance techniques, like DLTS, are very suitable for studies such as these, since the charge state can be easily controlled by the external bias that is applied.

In the case of figure 5.3 (c) and (d), the A configuration remains the stable configuration for both charge states. Conversion to the B configuration is still possible by using a technique like optical excitation or electrical injection.

The widely known cases of metastability of defects in semiconductors that have been reported up to know, are, for example, the interstitial carbon-substitutional carbon pair and the interstitial iron-acceptor pairs in silicon (Chantre 1989), the interstitial hydrogen in elemental and compound semiconductors (Watkins 1989), the ubiquitous EL2 defect in GaAs (Bois *et al* 1977 and Kaminska *et al* 1993), the DX centre in III-V and II-VI compound semiconductors and their alloys (Morgan 1991) and the M-centre in InP (Levinson *et al* 1983). Unfortunately for only a few of these cases has the defect been unambiguously identified and the mechanism for transformation between the different configurations been well established.

In GaAs, metastable defects have been observed in as-grown GaAs (Buchwald *et al* 1989), as well as in hydrogen- and deuterium-passivated epitaxially grown GaAs (Leitch *et al* 1991 and 1992). Electron irradiation induced metastable defects have been reported by Kol'chenko *et al* (1994) and Hesse *et al* (1994). An alpha-particle irradiation induced metastable defect has also been reported by Auret *et al* (1994).

Chapter 6: Thermodynamics of transformations

In this chapter a short overview is given of reaction kinetics, explaining certain terminology and how to determine what type of kinetics is involved from the data obtained. A more detailed discussion of reaction kinetics, particularly as they pertain to reactions of defects in semiconductors, is given by Bourgoin *et al* (1983).

6.1 First order reaction kinetics

Consider a reaction where the time evolution of a quantity N is given by the general equation

$$\frac{dN}{dt} = -KN^{\alpha} \tag{6.1}$$

where α is called the order of the reaction and K is the rate constant. If $\alpha = 1$, the reaction is said to be of first order and the decrease of the quantity N is proportional to the concentration of N. The kinetics of this reaction is then described by

$$N(t) = N_0 e^{-Kt} \tag{6.2}$$

where N_0 is the initial concentration of N. First order reaction kinetics in general describe processes where the diffusion of the reactant species plays the dominant role.

If a set of data that gives $N(t)$ as a function of time t has been obtained, the data can be tested for a relationship of the form of equation 6.2 by plotting a graph of ln $N(t)$ versus t. If the resulting plot is linear, then it can be said that the reaction under consideration has first order kinetics. From a straight line fit to the data points, the rate constant can calculated from the slope of the line and the initial concentration can be calculated from the intercept of the line at $t = 0$, which is ln N_0.

An example of first order reaction kinetics is the diffusion process of defects to sinks, where they react with the sinks and disappear.

An alternative form of equation 6.2 is given by

$$N(t) = N_0\left[1 - \exp(-Kt)\right] \tag{6.3}$$

which is still a solution of equation 6.1 with $\alpha = 1$, but in this case a plot of $\ln[\{N_0\text{-}N(t)\}/N_0]$ versus time t will give a linear plot.

6.2 Second order reaction kinetics

If $\alpha = 2$ in equation 6.1, the reaction is second order and the decrease of quantity N is proportional to the square of the concentration N. The reaction kinetics is described by

$$N(t) = \frac{N_0}{1 + N_0 Kt} \tag{6.4}$$

or in a different form

$$\frac{1}{N(t)} = \frac{1}{N_0} + Kt \tag{6.5}$$

where N_0 is the initial concentration and K is the rate constant.

If a set of data that gives $N(t)$ as a function of t has been obtained, the data can be tested for a relationship of the form of equation 6.4 by plotting a graph of $1/N(t)$ versus t. If the resulting plot is linear, then the reaction rate is second order and the relationship between $N(t)$ and t is given by equations 6.4 or 6.5. A straight line fit to the linear plot would yield the rate constant from the slope and the initial concentration from the intercept $1/N_0$.

Second order reaction kinetics in general describe processes where the energy barrier for the reaction of the reactants plays the dominant role, i.e. the kinetics are determined by the energy barrier, not by how the reactants came together (e.g. by diffusion).

An example of second order reaction kinetics is the annealing of two types of randomly distributed defects by direct recombination, for example in the case of vacancies and interstitials, created in equal numbers by irradiation and which recombine through a single jump.

6.3 The Arrhenius relation

It is often the case that the rate constant K in the previous paragraphs is temperature dependent, i.e. $K = K(T)$. This temperature dependence of the rate constant is given by the Arrhenius relation

$$K(T) = K_0 \exp(-\Delta E / kT) \tag{6.6}$$

where ΔE is an energy barrier, k is Boltzmann's constant and T is the absolute temperature.

In the case of defect annealing reactions in a semiconductor crystal, for example, ΔE is the energy barrier that the reactants must overcome before they can react and K_0 is referred to as the pre-exponential factor, or prefactor, of the rate constant. According to Chantre (1989), the

controlling mechanism for the reaction can be inferred from the value of the prefactor. The mechanisms which are consistent with an Arrhenius relation for the temperature dependence of the rate constant, are:

i. elementary atomic jump ($K_0 \sim 10^{12}$ s^{-1})
ii. free-carrier capture by multiphonon emission ($K_0 \sim 10^{7}$ s^{-1})
iii. free-carrier emission ($K_0 \sim 10^{13}$ s^{-1}).

The prefactor is related to the lattice vibration frequency ν_0 by (Lang 1977)

$$K_0 = \frac{\nu_0}{N_j} \exp(\Delta S / k) \tag{6.7}$$

where N_j is the average number of jumps required for the reactant to move before reaction takes place and ΔS is the entropy associated with the jump process.

The lattice vibration frequency is given by

$$\nu_0 \sim \frac{kT}{h} \tag{6.8}$$

where h is Planck's constant, so that at room temperature (300 K) $\nu_0 \sim 10^{12}$ s^{-1}. It is then reasonable to expect that for an elementary atomic jump $K_0 \sim 10^{12}$ s^{-1}, since in this case N_j is of order unity, as well as $\exp(\Delta S/k)$.

Chapter 7: Methodology

In this chapter the specific techniques and methodologies that were developed and used for this study, are described. The basic instrumentation used is given in the first section and the relevant detail changes are given in subsequent sections.

7.1 Instrumentation

The main instrumentation technique used in this study, was deep level transient spectroscopy (DLTS) first detailed by Lang (1974) and briefly described in chapter 4 of this dissertation. The instrumentation consisted of the following:

- closed cycle He cryostat (15K - 350K)
- Boonton model 7200 capacitance meter
- Stanford Electronics model SR 530 lock-in amplifier
- HP3245A constant current source
- HP PC with HP Vipercard running HPBASIC software

The above setup was available as a integrated setup at the beginning of this study, except for the HP3245A, which was incorporated into the system at the beginning of this study.

7.2 Sample details

Schottky-barrier diodes (SBDs) were used as the diode contact structure to the GaAs. The GaAs utilised consisted of a 5 μm thick layer doped to 1.1×10^{16} cm^{-3} with Si, grown by organometallic vapour-phase epitaxy (OMVPE) on a Si-doped n^+-GaAs substrate. Ohmic contacts were formed by depositing a Ni/AuGe/Au layer on the n^+-substrate and annealing it at 450°C. Thereafter 400 nm thick palladium contacts, 0.75 mm in diameter, were resistively deposited on the epitaxial layers to form SDBs.

The samples were irradiated with alpha-particles from a ^{241}Am radio nuclide source by placing the SBD Pd-side down in direct physical contact with the radio nuclide foil at room temperature (298K) and atmospheric pressure. The foil emits 5.4 MeV alpha-particles at a fluence rate of 7.1×10^6 $cm^{-2}s^{-1}$. The samples were irradiated for four hours to a total fluence of 1×10^{11} cm^{-2}.

Irradiation prior to SDB fabrication and irradiation after SDB fabrication was found to give the same DLTS spectra. The samples were placed in the cryostat after irradiation for subsequent measurements.

7.3 Transformation cycle

In the case of most metastable defects reported on so far, the transformation of the defect from a stable state to a metastable state and vice versa is brought about by a series of bias on / bias off annealing cycles, a typical description of which is given by Benton *et al* (1983).

A sample would be reverse biased, cooled to temperature T, then annealed under zero bias for a time t, followed by a DLTS scan which would show the defect in one of its states. The other state is observed by cooling the sample down to a temperature T under zero bias, annealing under reverse bias for a time t and then recording a DLTS scan. The DLTS peak associated with the first state is now smaller or has disappeared and a second peak, different from the first, is associated with the second state.

It was found that such transformation cycles were inadequate for the Eα3 defect. The application of a forward bias with the accompanying minority carrier injection was necessary at the annealing temperature T before the defect Eα3 could be induced to transform to its metastable state. A typical cycle was as follows: after cooling from 300 K to 20 K at a reverse bias of 2 V, a DLTS spectrum was recorded from 20 K to 300 K after first applying a strong forward current density of 5.6 A cm^{-2} at 105 K for a time t and subsequently cooling to 20 K.

The HP3245A was used to generate the conditions for minority carrier injection. Since it was difficult to quantify the current from the applied forward bias, because of unknown potential drops in the circuit, a constant forward current was applied instead of a constant forward bias.

Use was made of relays to switch the Boonton capacitance meter out of the circuit when the forward current was applied, because of its high internal impedance.

The forward current was also applied as a current pulse instead of a constant current. A current pulse I_p, width t_p was superimposed on a quiescent current I_r at a certain frequency such that the total forward current passing through the SBD in pulse form was the same as the total forward current passing through the diode in a single continuous application. This was done to minimise local heating effects in the sample due to resistive heating that may result in the sample temperature being different from the annealing temperature T measured in the cryostat. Typical values used, were I_p = 25 mA, I_r = 5 mA, t_p = 0.2 ms and frequency = 50 Hz.

Since the metastable behaviour of Eα3 depended critically on whether forward current flowed through the sample, it was verified that at no time during the annealing cycle did the switching of relays in the circuit cause any forward bias spikes that may effect the sample measurements detrimentally.

Chapter 8: Results

The results of the investigation into the electronic properties and the metastability of the defects Eα3 and Eα8, introduced in n-GaAs by alpha-particle irradiation, are presented here. The pertinent results are discussed as well and a model is suggested to explain the Eα3 behaviour.

8.1 Electronic properties of Eα3 and Eα8

Curve (a) in figure 8.1 is a typical DLTS spectrum of α-particle irradiated silicon doped n-GaAs and depicts the presence of the radiation-induced defects Eαl – Eα5 and Eα8. The electronic properties of these defects have been reported previously by Auret *et al* (1993b) and Goodman *et al* (1993) and it was shown that Eαl, Eα2 and Eα4 have the same DLTS signatures as the well-known electron irradiation induced defects El, E2 and E3, respectively, which in turn are related to vacancy - interstitial pairs in the As sublattice, as reported by Pons *et al* (1985). In this study we focus on the properties of defect Eα3 that exhibits a metastable character. From DLTS Arrhenius plots for Eα3, constructed from spectra for which the maximum electric field during emission was 3.2×10^4 V cm^{-1}, we calculated $E_t = E_c - 0.35$ eV and $\sigma_\infty = 9 \times 10^{-14}$ cm^2. Due to the larger field assisted emission, described by Lang *et al* (1975), in the doped GaAs used in this study, this signature is slightly different from that determined by Auret *et al* (1993b) and Goodman *et al* (1993) for the same defect in low doped n-GaAs. Variable pulse-width measurements, from Lang (1974), and using $V_r = 4$ V and $V_p = 4.2$ V, revealed that the electron capture cross-section of Eα3 is temperature dependent and changes from 3.0×10^{-19} cm^2 at 150 K to 1.6×10^{-18} cm^2 at 193 K. Figure 8.2 shows that electron capture by Eα3 is thermally activated according to:

$$\sigma(T) = \sigma_\infty \exp\left(-E_\sigma / kT\right) \tag{8.1}$$

where k is Boltzmann's constant and E_σ is the electron capture barrier. This temperature dependence of $\sigma(T)$ indicates that electron capture by Eα3 occurs by multiphonon emission [Lang *et al* 1975]. From figure 8.2 we calculated E_σ = (0.049±0.003) eV and $\sigma_\infty = (1.3 \pm 0.4) \times 10^{-15}$ cm^2. The capture barrier E_σ of Eα3 is smaller than the 0.10 eV reported by Lang *et al* (1975) for the E3 electron radiation induced defect which has the same DLTS

signature as Eα4 [Pons *et al* 1985 and Auret *et al* 1993b]. We attribute the lower value of σ_∞ calculated from figure 8.2, compared to that found from the DLTS Arrhenius plot for Eα3 to the higher maximum electric field (10^5 V cm^{-1}) present during the variable-temperature capture cross-section measurements.

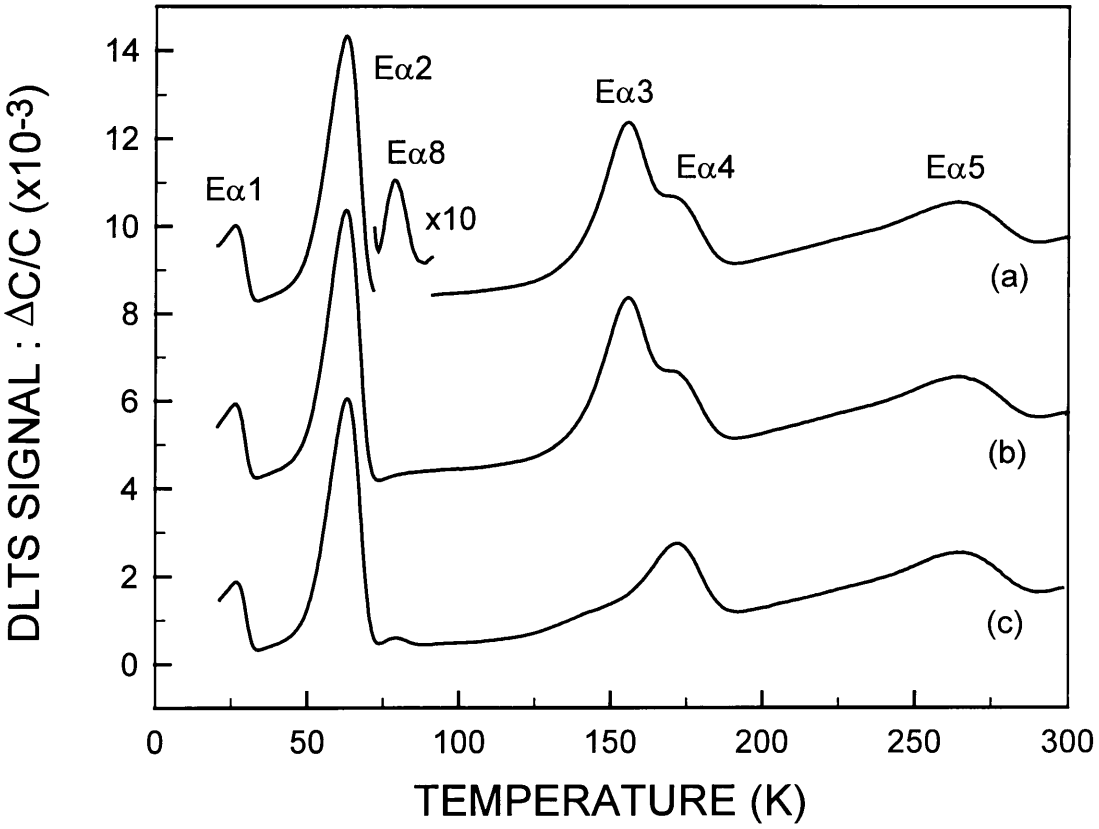

Figure 8.1: DLTS spectra of α-particle irradiated n-GaAs (f = 1 Hz, V_r = 2 V and V_p = 1.9 V): (a) after reverse bias (2 V) cooling; (b) after zero bias cooling; (c) after applying a forward current density of 5.6 A cm^{-2} at 105 K for 10 s.

The scan-up spectra (i.e. recorded from low to high temperature) in figure 8.1 indicate that the Eα3 concentration is strongly influenced by the previous scan-down bias as well as current-flow at low temperatures. In contrast, the peak heights of the other defects are independent of these conditions. Specifically, curves (a) and (b) reveal that Eα3 is present after reverse bias as well as zero bias cool down cycles, but that it is absent after applying a forward current density of 5.6 A cm^{-2} for 10 seconds at 105 K [curve (c)]. These bias- and current-induced transformations

of Eα3 are charge-state controlled and relate to a reversible disappearance and re-appearance of energy levels in the bandgap, thereby exhibiting charge state controlled metastability, as defined by Benton *et al* (1983). We assume this metastability is caused by transformations of Eα3 to and from states denoted by Eα3* for purposes of discussion.

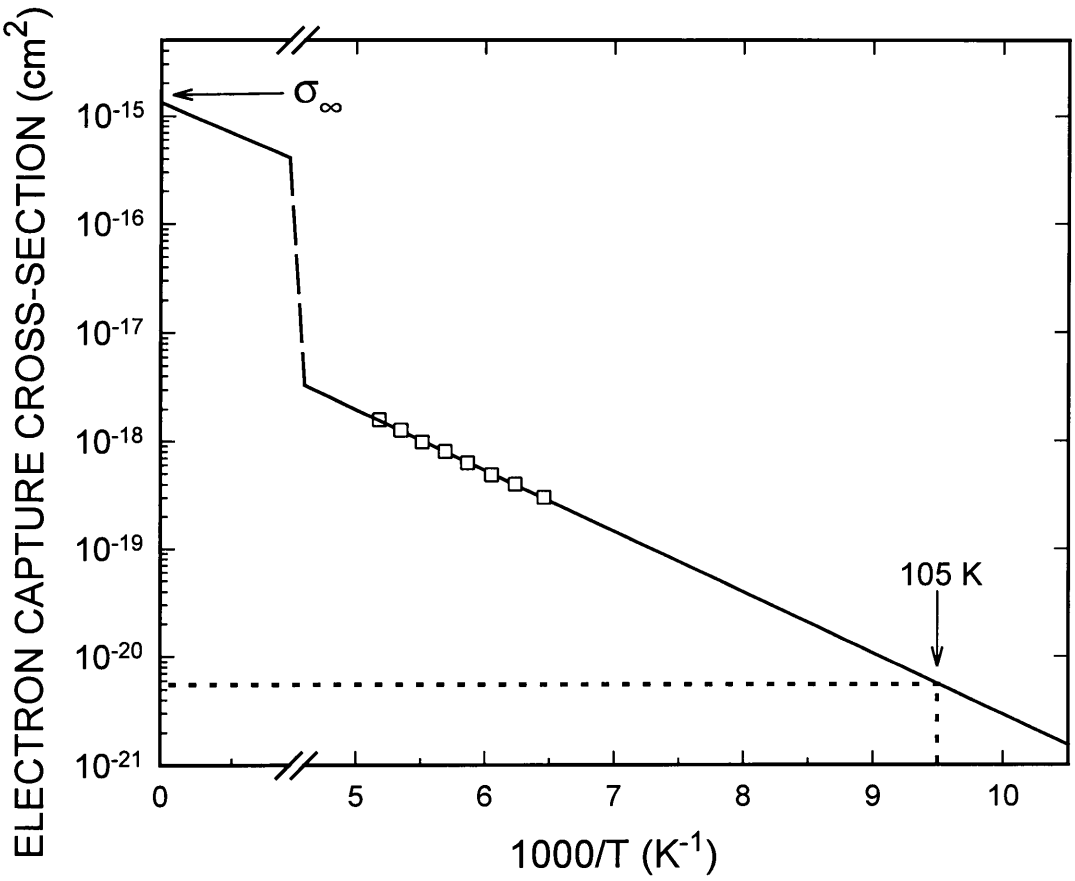

Figure 8.2: Variation of Eα3 electron capture cross-section as function of temperature. Measurement conditions: V_r = 4 V and V_p = 4.2 V.

The Eα8 defect has previously been reported by Goodman *et al* (1993) to have an energy level $E_t = E_c$ - 0.18 eV and an apparent capture cross section of 1×10^{-13} cm^2 in *n*-GaAs with a free carrier density of 1.1×10^{15} cm^{-3}. In this study, its activation energy and apparent capture cross section were found to be 0.16 eV and 1×10^{-14} cm^2, respectively, for the 10^{16} cm^{-3} doped GaAs used here, when applying bias and pulse conditions of $V_r = 2$ V and $V_p = 1.9$ V. The difference between the DLTS signatures determined here in GaAs with a higher carrier density and those in the previous study stems from the higher electric field during the present measurements than in

the previous study. This leads to an electric field assisted emission and consequently to a different DLTS signature, as was also the case with the Eα3 defect.

From the DLTS spectra, recorded in conjunction with bias-on / bias-off cooling cycles, given in figure 8.1, it is seen that the presence of the Eα8 peak is dependant on the bias applied during the cooling down cycle. Curve (a) shows the Eα8 defect present after the reverse bias cool down cycle, while curve (b) shows that Eα8 is removed during the zero bias cool down cycle. This reversible transformation behaviour of Eα8 characterises it as a metastable defect with at least two configurations: the Eα8, which is commonly observed in irradiated GaAs, and another that we shall refer to as Eα8*.

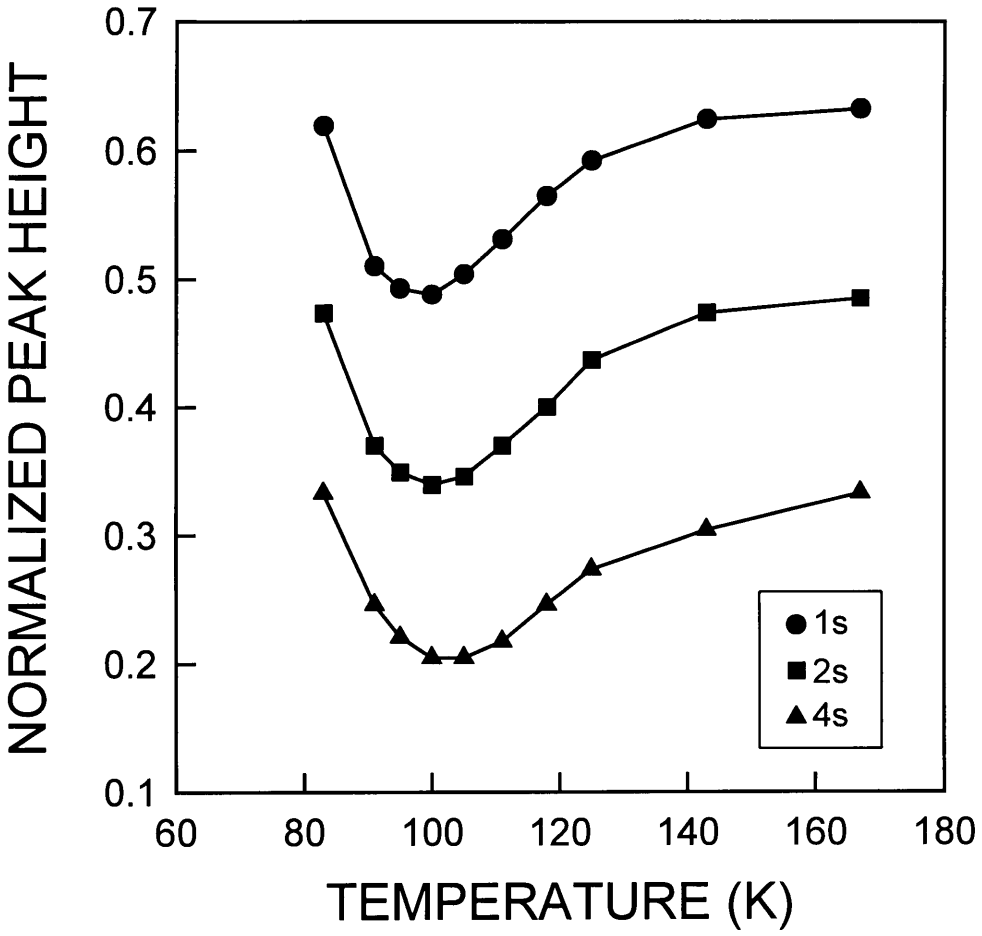

Figure 8.3: Change in Eα3 peak height as a function of temperature when a forward current is applied at a current density of 1.4 A cm^{-2} for times 1 s, 2 s and 4 s.

8.2 Metastable character of the Eα3 defect

We consider the transformation of Eα3. The results obtained after isochronally annealing Eα3 during the flow of current, are illustrated in figure 8.3. For a given current density each isochronal curve shows an increasing transformation rate Eα3 → Eα3* as temperature increases from 80 K to 100 K. There is a clear optimum temperature, similar for 1s, 2s and 4s, around 105 K, at which the Eα3 → Eα3* transformation is most successful. As the temperature increases further, the transformation rate slows down again until it is about the same at 167 K as at 83 K.

This Eα3 removal can be explained qualitatively in terms of hole injection: The minority carrier injection ratio into the depletion region of a SBD is small but finite, and it increases with increasing forward current density [Scharfetter 1965]. Thus, when applying a large enough forward bias, it is possible to introduce holes into the depletion layer of a SBD. Minority carrier injection in SBDs was used to detect hole traps in n-GaAs by DLTS [Auret *et al* 1988]. In the present study, holes injected into the depletion region at 105 K during forward pulsing are trapped by Eα3 or another level belonging to the same defect. At 105 K the Eα3 electron capture cross-section is estimated from figure 8.2 as $< 5 \times 10^{-21}$ cm^2, signifying that its electron capture rate at 105 K is less than 2×10^2 s^{-1}. We propose that after hole capture, Eα3 transforms to Eα3* with an energy level different to Eα3 - illustrated by the decrease in the Eα3 DLTS signal.

Thermally stimulated capacitance (TSCAP) curves - where the capacitance, C, is recorded as a function of increasing temperature, T - are presented in figure 8.4. They show that the total positive charge in the depletion layer is higher after the forward current pulse sequence at 105 K than after cooling to 105 K at zero bias. This indicates that either electron emission to the conduction or valence band (hole capture) takes place during the current pulse cycle at 105 K. Furthermore, during the TSCAP heating cycle, after the transformation sequence at 105 K, a decrease in $\Delta C/\Delta T$ occurs in the 170 K–200 K temperature range - the same range in which the Eα3* → Eα3 transformation occurs. A decrease in $\Delta C/\Delta T$ with increasing T can be the result of either electron capture from the conduction band or otherwise, hole emission to the valence band. However, since all TSCAP curves were recorded under reverse bias, almost no free electrons are available for capture. This signifies that the decrease in $\Delta C/\Delta T$ between 170 K and 200 K is caused by hole emission. Therefore, our TSCAP results imply that the Eα3 transformations are related to hole capture and emission.

Semi-transparent Au-SBDs were used to qualitatively investigate the response of the Eα3 defect to optical stimuli. The sample was illuminated through the SBD with a laser diode, energy

1.45 eV. The sample was cooled from 300 K to 20 K under a reverse bias of 2V and a DLTS spectrum was

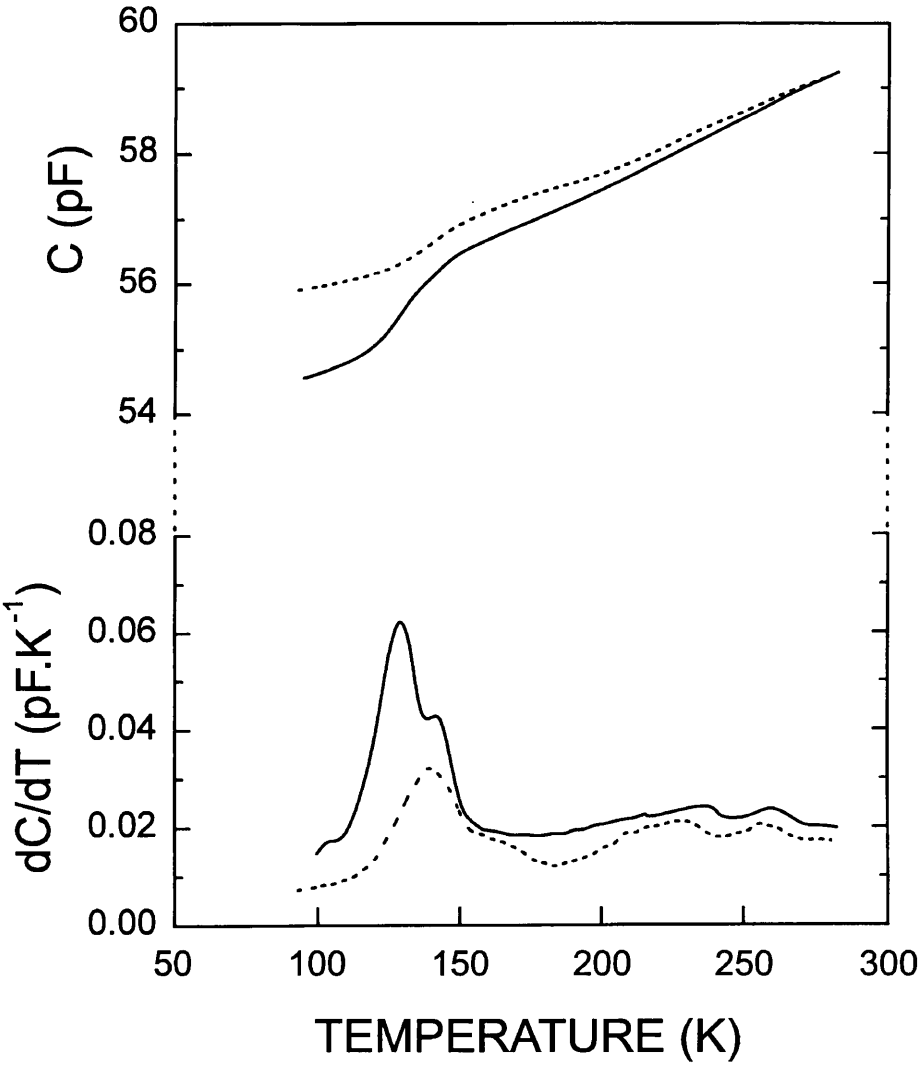

Figure 8.4: TSCAP (C vs. T) and dC/dT vs. T of OMVPE grown 1.1 × 10^{16} cm^{-3} doped n-GaAs, irradiated with alpha-particles. The capacitance was recorded at a scan rate of 3 K min^{-1}.

——— *Zero bias cooldown, then scan up with* V_r *= 4 V.*

--------- *Zero bias cooldown followed by the application of an injection pulse, then scan up with* V_r *= 4 V.*

recorded from 20 K to 300 K with the light source flashing in phase with the DLTS voltage pulse V_p. The resultant spectrum showed the same main feature as [figure 8.1, curve (c)], namely the absence of the Eα3 peak. Holes are available via the electron-hole pairs generated by the optical

pulse and are subsequently captured by Eα3 and it transforms to Eα3*, disappearing from the DLTS spectrum.

The free carrier density in the Pd-SBD sample was also determined at 140 K by capacitance-voltage (C-V) measurements before and after the current pulse sequence. From this it was found that there was an increase in free carrier density after the current pulse sequence up to 0.8 μm from the interface. The change in free carrier density, i.e. an increase of 2×10^{14} cm^{-3}, is very similar to the concentration of the Eα3 defect, namely 2.4×10^{14} cm^{-3}. This further strengthens the case for hole capture by Eα3, since the number of free carriers gained after the defect was transformed to Eα3*, is the same as the number of Eα3 defects that compensated these carriers when it was present.

As mentioned, the isochronal annealing characteristics of the transformation Eα3 → Eα3* is illustrated in figure 8.3. In the temperature range 80 K to 100 K, plots of $N_T / N(t)$ vs. time (t) at different temperatures (N_T is the total Eα3 concentration) were straight lines, indicating that the transformation obeys second order kinetics described by

$$1 / N(t) = 1 / N_T + \nu(T)t \qquad (8.2)$$

Here $N(t)$ is the occupied Eα3 concentration and $\nu(T)$ is the introduction rate-constant at temperature T. From Arrhenius plots of $\ln[\nu(T)]$ vs. $1/T$, the temperature dependency of the removal rates over the specified temperature range were found to obey the relation

$$\nu(T) = \nu_0 \exp(-\Delta E / kT) \qquad (8.3)$$

where ΔE is the energy barrier for the Eα3 removal. From the ν_o and ΔE values so calculated, the Eα3 → Eα3* transformation can be summarised as:

$$\text{Eα3} \rightarrow \text{Eα3}^*: \quad \nu(T) = 2.14 \times 10^4 \exp(0.041 / kT)$$

The rate constant (2.14×10^4 s^{-1}) is much smaller than that expected for carrier capture, namely $\nu_o \sim 10^7$ s^{-1} [Auret *et al* 1993a]. Since a capture process is the rate limiting factor, the expression $\sigma_p p \upsilon_{th}$ dominates the rate constant, where σ_p is the hole capture cross section, p the minority carrier concentration and υ_{th} the hole thermal velocity. The discrepancy can then be explained by the very small minority carrier concentration p compared to the majority carrier concentration in the n-type GaAs.

Isochronal annealing indicated that Eα3 is reintroduced at temperatures above 160 K under zero bias, or above 190 K under reverse bias, and from isothermal annealing in these temperature ranges we obtained the Eα3* → Eα3 transformation kinetics. Plots of $\ln[\{N_T - N(t)\}/N_T]$ vs.

time (t) at different temperatures were straight lines, indicating that the transformation obeys first-order kinetics described by

$$N(t) = N_T\left[1 - \exp\{-\nu(T)t\}\right] \qquad (8.4)$$

This equation has also been found to describe the introduction rates of hydrogen-related metastable defects in OMVPE grown GaAs [Buchwald *et al* 1989]. From Arrhenius plots of $\ln[\nu(T)]$ vs. $1/T$ the temperature dependencies of the zero- and reverse bias introduction rates were both found to obey the relation 8.3, where ΔE is the energy barrier for the Eα3 formation. From the ν_o and ΔE values thus calculated, the Eα3* → Eα3 transformations can be summarised as:

Eα3* → Eα3: $\nu = (6 \pm 2) \times 10^8 \exp\left[-(0.40 \pm 0.01)/kT\right]$ (zero bias)

$\nu = (6 \pm 2) \times 10^9 \exp\left[-(0.53 \pm 0.01)/kT\right]$ (2 V reverse bias)

The rate constants above are smaller than expected for carrier emission, but slightly larger than expected for carrier capture [Auret *et al* 1993a]. However, since the Eα3 → Eα3* process resulted from hole capture, it is reasonable to expect that the opposite process (Eα3* → Eα3) stems from hole emission, as suggested by our TSCAP data. The activation barrier for the transformation under zero-bias is ΔE = (0.40±0.01) eV, which is lower than the ΔE = (0.53±0.01) eV of the process under reverse bias. The lower ΔE measured under zero bias supports the model of hole release, i.e. electron capture, since at zero bias there is an abundance of electrons.

This phenomenon of accelerated re-introduction of a defect in the presence of electrons, shows a qualitative resemblance to the so-called Auger de-excitation of the optically activated metastable state of the EL2 defect in n-GaAs [Mitonneau *et al* 1979]. Here it was found that the transition from the metastable state to the stable state was much enhanced in the presence of free electrons, although in the case of Eα3 it would involve an electron-hole interaction.

A configuration-coordinate (C-C) diagram of the Eα3 defect encompassing the results presented in this paper, is suggested in figure 8.5. The positions of the Eα3 and Eα3* levels relative to the conduction band and valence band, are shown. The energy barrier for the transition from Eα3 to Eα3* is 0.041 eV and for the reverse transition 0.40 eV. A large degree of lattice relaxation on the part of Eα3* is implied by the observed results.

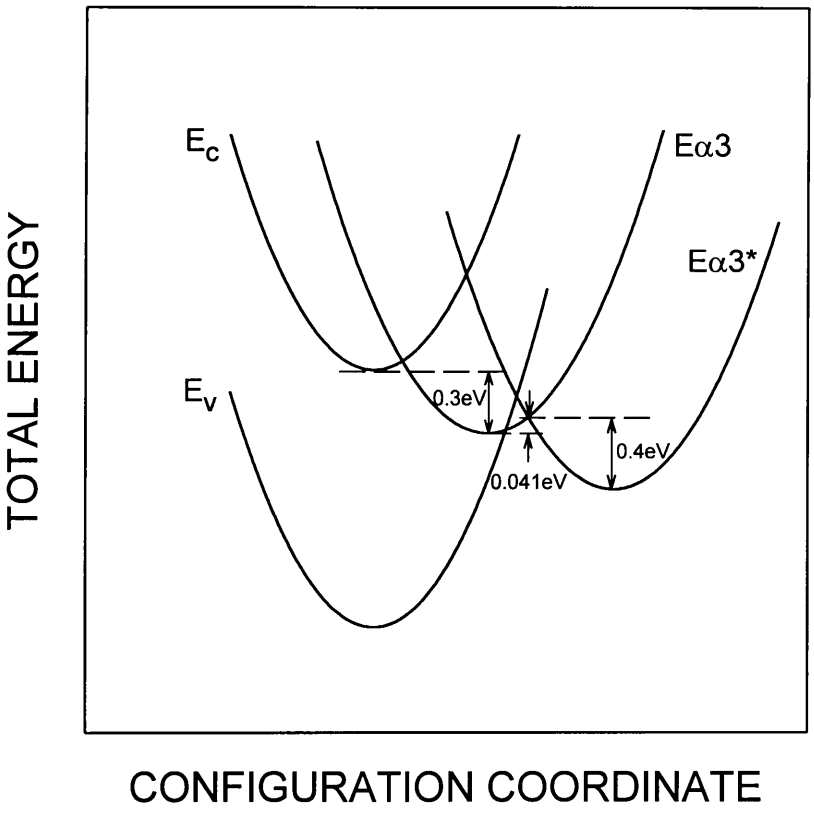

Figure 8.5: Configuration-coordinate (C-C) diagram for the Eα3 defect

Although DLTS does not provide information about the physical nature of defects, we nevertheless have two clues as to what Eα3 may consist of. Firstly, Eα3 is present in higher concentrations in GaAs doped to 10^{16} cm^{-3} with Si used here than in undoped GaAs previously investigated. Secondly, Eα3 is observed in alpha-particle irradiated GaAs but not in electron irradiated GaAs with the same dopant and carrier concentration. Since an alpha-particle can transfer much more energy to the lattice than an electron with the same kinetic energy, it is capable of forming disordered regions with a larger extent than the simple point defects typically observed after electron irradiation.

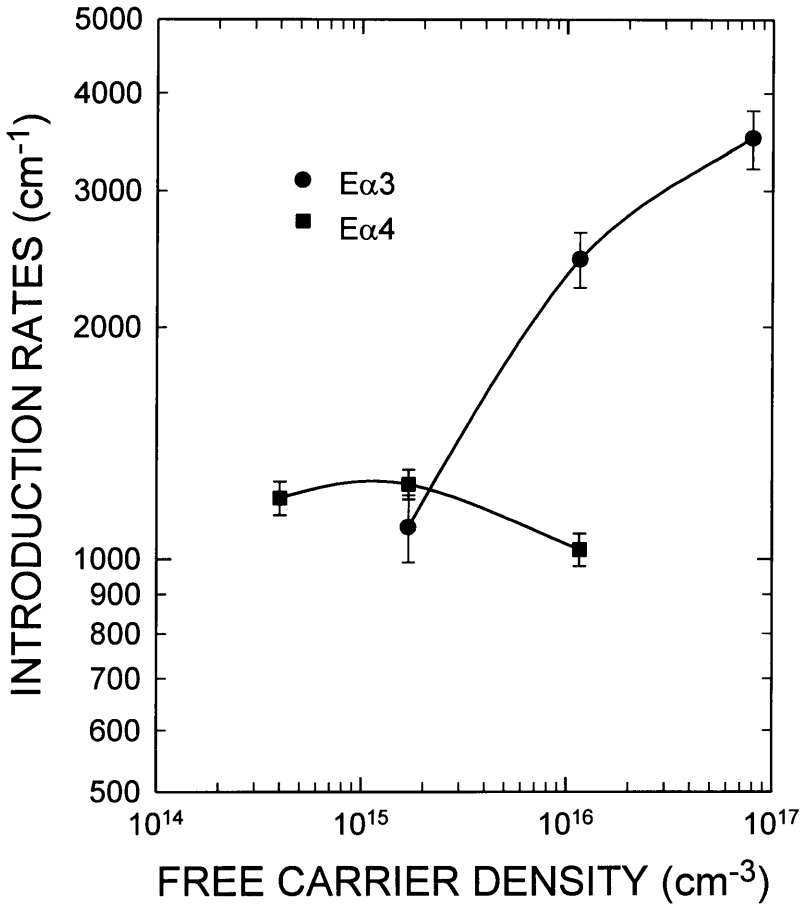

Figure 8.6: Change in Eα3 and Eα4 introduction rates as a function of free carrier concentration for Si-doped n-GaAs.

In figure 8.6 the relationship between Eα3 and Eα4 introduction rates and free carrier density for Si-doped material is presented. It is clear that for the same fluence of alpha particles, there is a higher introduction rate of Eα3 in material doped to a higher level, illustrating a relationship between Eα3 and Si concentration. Introduction rates of the other defects Eα1, Eα2, Eα4, Eα5 and Eα8 stay constant with increasing free carrier density, as typically illustrated by Eα4. The apparent decrease in the introduction rate of Eα4 for 10^{16} cm^{-3} free carrier density material is due to the high electric field dependence of this defect, as reported by Goodman *et al* (1994), resulting in a smaller measured peak height. It has also been found that in material doped to the same levels as in figure 8.6 with different doping materials no presence of Eα3 could be found

after alpha-particle irradiation. In view of these facts we suggest that Eα3 may consist of a Si atom linked to a more complex lattice defect than an As vacancy or interstitial.

8.3 Metastable character of the Eα8 defect

As indicated, Eα8 is a defect that exhibits metastable characteristics. In order to identify the temperature range in which the transformations from Eα8 to Eα8* and back occurred, five minute isochronal anneal cycles at 10 K intervals were performed, both under zero and reverse bias conditions. This was realised by cooling from above 200 K at one bias condition, (e.g. reverse bias) to a temperature T, then changing the bias condition (e.g. to zero bias) and maintaining the sample at this temperature for five minutes, followed by rapid cooling to 20 K under the same bias conditions as employed for the anneal. The data thus obtained shows that the Eα8 is introduced during reverse bias annealing in the 120 - 140 K range and removed during zero bias annealing in the 100 - 120 K range.

Isothermal annealing in the above mentioned temperature ranges was employed to calculate the introduction and removal rates, respectively, as a function of temperature. For the introduction rate of Eα8, plots of $\ln[\{N_T - N(t)\}/N_T]$ vs. time, t, at different temperatures (where N_T) is the total Eα8 concentration) yielded straight lines. This implies that the density of occupied Eα8 sites, $N(t)$, is given by

$$N(t) = N_T\left[1-\exp\{-\nu(T)t\}\right] \tag{8.5}$$

where $\nu(T)$ is the introduction rate constant at temperature T. Therefore, the introduction transformation Eα8*→Eα8 follows first order kinetics governed by the equation

$$dN(t)/dt = \nu(T)\left[N_T - N(t)\right] \tag{8.6}$$

This equation is typical for defect transformation and has also been used to calculate the introduction rates of hydrogen related metastable defects in OMVPE grown GaAs [Buchwald *et al* 1989]. From a conventional Arrhenius plot, the temperature dependence of the reaction rate was seen to follow the relation

$$\nu(T) = \nu_0 \exp\left(-\Delta E / kT\right) \tag{8.7}$$

where ΔE is the energy barrier for the transformation (formation in this case) of Eα8 and k is Boltzmann's constant. The prefactor ν_o and ΔE were determined as 4×10^{12} s^{-1} and 0.41 eV, respectively. The value of ν_o is of the same order of magnitude as that associated with free carrier emission [Chantre 1989]. Hence we deduce that Eα8 is formed when the Eα8* configuration, with an energy level deeper in the bandgap than Eα8, emits an electron to the conduction band.

The removal transformation of Eα8 also follows first order kinetics, satisfying the relation

$$N(t) = N_T \exp\{-\nu(T)t\}, \tag{8.8}$$

which is a solution of

$$dN(t)/dt = -\nu(T)N(t) \tag{8.9}$$

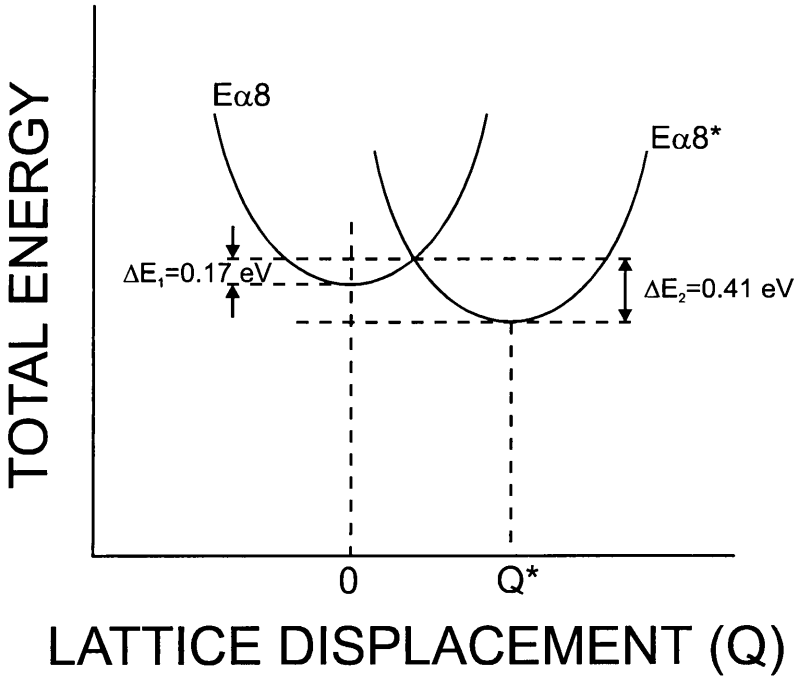

Figure 8.7 Configuration coordinate (CC) diagram depicting the total (elastic+electronic) energy of the defect as a function of lattice configuration coordinate Q for the two configurations Eα8 and Eα8.*

In this case $\nu(T)$ represents the removal rate constant of Eα8. The prefactor ν_o and reaction energy barrier ΔE for Eα8 removal were calculated as 4×10^4 s^{-1} and 0.17 eV, respectively. The low value of ν_o together with the fact that the removal of Eα8 occurs under zero bias, i.e. when it lies below the Fermi level, indicates that the transformation is the result of electron capture: upon electron capture in the temperature range 100 - 120 K, Eα8 undergoes a configurational change to become Eα8* with an energy level deeper in the bandgap.

The results above can be summarised by the configuration coordinate diagram in figure 8.7. After a reverse bias cool down the defect is in configuration Eα8 of which the total energy parabola in the CC diagram has a minimum at Q=0. In order for Eα8 to be transformed to the Eα8* configuration, it has to be occupied (zero bias applied) and the temperature has to be high enough

so that the change in Q is sufficient to enable the electron to surmount the transformation barrier ΔE_1. Thus Eα8 transforms to Eα8* and the electron is trapped in a deeper potential well. Such a configurational transformation is characterised by another parabola in the CC diagram with a minimum energy at Q=Q^*. In order for the reverse transformation (Eα8*→Eα8) to take place, the barrier ΔE_2 has to be overcome and since ΔE_2>ΔE_1 this transformation occurs at a higher temperature than the Eα8→Eα8* transformation.

Chapter 9: Conclusions

In this dissertation the metastable character of two alpha-particle irradiation induced defects in n-GaAs, Eα3 and Eα8, was investigated and reported. The following conclusions can be made:

The results presented here indicate that the alpha-particle irradiation induced a defect in n-GaAs, Eα3, which exhibits charge-state controlled metastability and can be reversibly transformed using conventional bias-on / bias-off temperature cycles in conjunction with forward current hole injection pulses at specific temperatures. The Eα3 has an energy level 0.35 eV below the conduction band and a thermally activated capture cross-section [capture barrier $E_\sigma = (0.049 \pm 0.003)$ eV], indicating that electron capture occurs by multiphonon emission. From its electronic properties and concentration it is clear that Eα3 can significantly assist radiation induced carrier removal. Under hole injection - obtained using SBDs - Eα3 transforms to Eα3* in the temperature range 80 K to 160 K, while under zero as well as reverse bias Eα3* transforms back to Eα3 by hole emission in the temperature range 160 K to 190 K. This metastable behaviour of Eα3 may either result in unstable, or if properly taken advantage of, tuneable device characteristics. The energy levels of Eα3* could not be detected by DLTS measurements, since its large lattice relaxation moves it to a position where the energy transition to the conduction band is too large for DLTS to detect it, because the DLTS peak temperature is around 250K, which is much higher than the Eα3* $\rightarrow$ Eα3 transformation temperature interval of 160 K to 190 K. This is illustrated in the proposed C-C diagram (figure 8.5).

It has been shown by Goodman *et al* (1994) that is possible to permanently remove the Eα3 defect by means of thermal annealing at a temperature of 513 K in a high purity argon atmosphere for two hours.

The Eα8 alpha-particle irradiation induced defect is a less prominent defect than Eα3 and can be reversibly transformed using conventional bias-on / bias-off temperature cycles. The Eα8 has an energy level 0.16 eV below the conduction band and an apparent capture cross section of 1×10^{-14} cm^2. Data presented show that the Eα8* transforms to Eα8 during reverse bias annealing

in the 120 - 140 K temperature range and the reverse transformation ($E\alpha 8 \rightarrow E\alpha 8^{*}$) takes place during zero bias annealing in the 100 - 120 K temperature range.

The physical nature of these defects can presently at best be speculated about but the existing evidence suggests that the presence of $E\alpha 3$ depends on the dopant used and on the GaAs free carrier concentration and that it requires a larger energy of formation than primary electron irradiation-induced defects.

9.1 Suggestions for future studies

- During the investigations reported on in this dissertation, it was noted that the introduction rate of $E\alpha 3$ in irradiated n-GaAs was strongly time dependent. This was investigated and the results were presented at IBMM Australia 1995 by Auret *et al* (1995).
- Investigation of the response of $E\alpha 3$ to optical stimuli and the subsequent determination of variables such as the photocurrent, absorption function and optical capture cross sections, would yield further clues to the nature of the $E\alpha 3$ defect.
- Since electrical and optical measurements only focus on the behaviour of defects, specific techniques designed to probe structure, such as ODEPR, ED-EPR, ODMR and double resonance techniques (ENDOR) are necessary to verify the speculations regarding the structure of $E\alpha 3$. Some of these studies could possibly be carried out by Dr. S.A. Goodman when he visits at the University of Paderborn in Germany during 1996.

References

Allen L C 1955 Interpolation Scheme for Energy Bands in Solids *Phys. Rev.* **98** 993

Auret F D, Nel M and Leitch A W R 1988 A comparison of deep level defects in OMVPE GaAs layers grown on various GaAs substrate types *J. Cryst. Growth* **89** 308

Auret F D, Goodman S A, Hayes M, Barnard W O and Meyer W E 1993a Electrical characterization of particle-induced damage in n-GaAs *S. Afr. J. Phys.* **16** 153

Auret F D, Goodman S A, Myburg G and Meyer W E 1993b Electrical characterization of defects introduced in *n*-GaAs by alpha and beta irradiation from radionuclides *Appl. Phys. A* **56** 547

Auret F D, Erasmus R M and Goodman S A 1994 A Metastable Alpha-Particle Irradiation Induced Defect in n-GaAs *Jpn. J. Appl. Phys.* **33** L491

Auret F D, Goodman S A, Erasmus R M, Meyer W E and Myburg G 1995 Electronic and annealing properties of a metastable He-ion implantation induced defect in GaAs *Nucl. Instr. and Meth. in Phys. Res.* **B106** 323

Bardeen J 1947 Surface States and Rectification at a Metal Semi-Conductor Contact *Phys. Rev.* **71** 717

Benton J L and Levinson M 1983 In *Defects in Semiconductors II* (New York: North-Holland) p.95

Bois D and Vincent G 1977 Mise en évidence d'un état métastable du centre associé a l'oxygène dans GaAs *J. Phys. Lett. (F)* **38** 351

Bourgoin J and Lannoo M 1983 *Point Defects in Semiconductors II: Experimental Aspects* (Berlin: Springer-Verlag)

Bourgoin J C and von Bardeleben H J 1986 Native defects in gallium arsenide *J. Appl. Phys.* **64** R65

Buchwald W R, Gerardi G J, Pointdexter E H, Johnson N M, Grimmeiss H G and Keeble D J 1989 Electrical and optical characterization of metastable deep-level defects in GaAs *Phys. Rev. B* **40** 2940

Chantre A and Kimerling L C 1986 Configurationally multistable defect in silicon *Appl. Phys. Lett.* **48** 1000

Chantre A 1989 Introduction to Defect Bistability *Appl. Phys. A* **48** 3

Goodman S A and Auret F D 1993 Deep Level Transient Spectroscopy Characterization of Defects Introduced in n-GaAs after Alpha Irradiation at 15K *Jpn. J. Appl. Phys. Lett.* **32** L1120

Goodman S A, Auret F D and Myburg G 1994 Defect Annealing of Alpha-Particle Irradiated n-GaAs *Appl. Phys. A* **59** 305

Goodman S A 1994 *Influence of Particle Irradiation on the Electrical and Defect Properties of GaAs* (PhD Thesis: University of Pretoria)

Herman F 1955 The Electronic Energy Band Structure of Silicon and Germanium *Proc. IRE* **43** 1703

Hesse M, Koschnick F K, Krambrock K and Spaeth J-M 1994 Metastability of arsenic antisite-related defects created by electron-irradiation in Gallium Arsenide *Sol. St. Comm.* **92** 207

Kaminska M and Weber E R 1993 *Semiconductors and Semimetals Vol.38* (New York: Academic Press)

Kol'chenko T I and Lomakoi V M 1994 New metastable center in electron-bombarded GaAs *Semiconductors* **28** 501

Lannoo M and Bourgoin J 1981 *Point Defects in Semiconductors I: Theoretical Aspects* (Berlin: Springer-Verlag)

Lang D V 1974 Deep-level transient spectroscopy: A new method to characterize traps in semiconductors *J. Appl. Phys.* **45** 3014

Lang D V 1977 Review of radiation-induced defects in III-V compounds *Inst. Phys. Conf. Ser. No. 31* 70

Lang D V and Henry C H 1975 Nonradiative Recombination at Deep Levels in GaAs and GaP by Lattice-Relaxation Multiphonon Emission *Phys. Rev. Lett.* **35** 1525

Leitch A W R, Presca Th and Weber J 1991 Negatively charged hydrogen species in *n*-type GaAs *Phys. Rev. B* **44** 1375

Leitch A W R, Presca Th and Weber J 1992 Hydrogen-related metastable defects in passivated *n*-type GaAs grown by metal-organic vapor-phase epitaxy *Phys. Rev. B* **45** 14400

Levinson M, Stavola M, Benton J L and Kimerling L C 1983 Metastable *M* center in InP: Defect-charge-state–controlled structural relaxation *Phys. Rev. B* **28** 5848

Miller G L, Lang D V and Kimerling L C 1977 Capacitance Transient Spectroscopy *Ann. Rev. Mater. Sci.* 377

Mitonneau A and Mircea A 1979 Auger de-excitation of a metastable state in GaAs *Sol. St. Comm.* **30** 157

Morgan T N 1991 The DX centre *Semicond. Sci. Technol.* **6** B23

Mott N F 1938 Note on the Contact between a Metal and an Insulator or Semiconductor *Proc. Cambr. Philos. Soc.* **34** 568

Phillips L C 1958 Energy-Band Interpolation Scheme Based on a Pseudopotensial *Phys. Rev.* **112** 685

Pons D and Bourgoin J C 1985 Irradiation-induced defects in GaAs *J. Phys. C: Solid State Phys.* **18** 3839

Rhoderick E H and Williams R H 1988 *Metal-Semiconductor Contacts 2nd ed.* (Oxford: Clarendon Press)

Scharfetter D L 1965 Minority carrier injection and charge storage in epitaxial Schottky barrier diodes *Solid-State Electron.* **8** 299

Schottky W 1938 Halbleitertheorie der Sperrschicht *Naturwissenschaften* **26** 843

Shockley W and Read W T Jr. 1952 Statistics of the Recombinations of Holes and Electrons *Phys. Rev.* **87** 835

Smith R A 1979 *Semiconductors 2nd ed.* (London: Cambridge University Press)

Sze S M 1981 *Physics of Semiconductor Devices 2nd ed.* (New York: John Wiley & Sons)

Watkins G D 1989 Defect metastability and bistability *Materials Science Forum* **38-41** 39